A Dynamic Regional Integrated Assessment Model to Assess the Impacts of Changing Globalization and Environmental Stewardship on the Regional Economy and Environmental Quality

Junyoung Jeong, The Ohio State University, jeong.352@osu.edu
Brian Cultice, The Ohio State University, cultice.7@osu.edu
Soomin Chun, National Renewable Energy Laboratory, chun.170@osu.edu
C. Dale Shaffer-Morrison, University of Essex, dale.shaffer-morrison@essex.ac.uk
Ziqian Gong, North Carolina State University, zgong5@ncsu.edu
Jeffrey Bielicki, The Ohio State University, bielicki.2@osu.edu
Yongyang Cai, The Ohio State University, cai.619@osu.edu
Elena Irwin, The Ohio State University, irwin.78@osu.edu
Douglas Jackson-Smith, The Ohio State University, jackson-smith.1@osu.edu
Jay Martin, The Ohio State University, martin.1130@osu.edu
Robyn Wilson, The Ohio State University, wilson.1376@osu.edu

Invited Paper prepared for presentation at the **2024 AEA/ASSA Annual Meeting, January 5-7, 2024, San Antonio, TX**

A Dynamic Regional Integrated Assessment Model to Assess the Impacts of Changing Globalization and Environmental Stewardship on the Regional Economy and Environmental Quality*

Junyoung Jeong[†], Brian Cultice[†‡], Soo Min Chun[§], C. Dale Shaffer-Morrison[¶], Ziqian Gong[‖], Jeffrey Bielicki[†], Yongyang Cai[†], Elena Irwin[†], Douglas Jackson-Smith[†], Jay Martin[†], Robyn Wilson[†]

December 18, 2023

Abstract

Changes in the global economy and climate system have large and wide-ranging repercussions for local and regional economies and ecosystems. Here we focus on global-to-local linkages that are hypothesized to impact water quality outcomes within a five-state Great Lakes-Corn Belt region, which includes some of the most intensive agricultural region of the Midwest. We develop a dynamic integrated assessment model (IAM) that links the regional economy to global conditions, local land use change, and water quality outcomes and use a scenarios framework to assess the likelihood that phosphorus reduction targets for Lake Erie are met by 2050 under a range of plausible global and regional conditions. We examine the relative role that global economic and climate conditions play in regional land use and water quality

*We acknowledge support from the National Science Foundation grant SES-1739909 and USDA NIFA-AFRI grant 2018-68002-27932.

[†]The Ohio State University
[‡]U.S. Energy Information Administration
[§]National Renewable Energy Laboratory
[¶]University of Essex
[‖]North Carolina State University

outcomes and the extent to which local land stewardship incentives and best management practices (BMPs) can offset the potential negative effects of global economic and environmental changes. By integrating a regional-level forward-looking dynamic model, a state-level static computable general equilibrium model, and a local-level land use change model, this IAM enables a comprehensive and theoretically consistent integration from global conditions through regional and local decision-making. The model simulates five scenarios defined by distinctly different combinations of global commodity prices, CO_2 prices, climate conditions, productivity, population, and economic growth. Our results reveal that success in attaining the policy target is relatively uncertain and highly dependent on future economic, environmental, and policy conditions. We find that only two of the scenarios are projected to attain the 40 percent spring DRP and TP reduction targets nine out of ten years by the 2030's. Other results confirm that lower commodity prices generally lead to reduced cropland acres and are mostly associated with better water quality outcomes. However greater intensification of cropland use is not associated with greater water pollution, a result that may be driven by the relatively high adoption rates for subsurface placement that are reached in later years across scenarios. Taken together, these results demonstrate the potential for local policies to incentivize BMP adoption at levels that can act as a buffer to uncertain, changing global conditions.

Keywords: food-water-energy systems, integrated assessment model, global-to-local linkages, scenarios framework, global economy, environmental stewardship, climate change

1 Introduction

Changes in the global economy and climate system have large and wide-ranging repercussions for local and regional economies and ecosystems. In the recent U.S.-China trade war, for example, greater trade barriers to U.S. producers reduced U.S. exports and lowered commodity prices (Regmi, 2019), which altered the relative net returns to cropland at a field level. Allocations of U.S. cropland shifted (Lee et al., 2023) and, depending on regional conditions, the amount of land allocated to other uses—pasture, conservation, forests, urban—may have also shifted with conse-

quent impacts on water quality, biodiversity, carbon sequestration, and other ecosystem services. While multi-sector interactions across economic, climate, and other system are well-studied at the global and national scales, the implications of changing global conditions for local and sub-national economic and environmental outcomes are less understood (Hertel et al., 2023). This is due to the complexity of cross-scale interactions and the need for considerably more model detail, including spatially explicit and heterogeneous representations of land use decision making, at local and regional scales. Incorporating these details is critical for assessing the local consequences of global change and accounting for these interdependencies in guiding local and regional policies to efficiently allocate land to productive uses while protecting habitat, water, and other critical forms of natural capital.

In this paper, we focus on global-to-local linkages that are hypothesized to impact water quality outcomes within a five-state Great Lakes-Corn Belt region, which includes some of the most intensive agricultural region of the Midwest. We use a scenarios framework to assess the likelihood that phosphorus reduction targets for Lake Erie are met by 2050 under a range of plausible global and regional conditions. We examine the relative role that global economic and climate conditions play in regional land use and water quality outcomes and the extent to which local land stewardship incentives, currently represented in our model via payments for agricultural land conservation and best management practices, can offset the potential negative effects of expanding global commodity markets or worsening climate change. To link global economic and environmental conditions with local and regional land use and water quality changes, we develop a **D**ynamic **R**egional **F**ood-**E**nergy-**W**ater **S**ystems (DRFEWS) integrated assessment model (IAM). The key methodological innovation of DRFEWS lies in the integration of five sub-models. We formulate the dynamic interactions between 1) a regional-level forward-looking dynamic model, 2) a state-level static computable general equilibrium (CGE) model, both specified with a detailed representation of agriculture, food, energy, transportation, and manufacturing sectors, 3) a local-scale land use change model that accounts for spatial heterogeneity in soil quality and economic conditions, and 4) a farmer management model that describes individual heterogeneity in agricul-

tural land management practices. This enables a theoretically consistent integration from global conditions through individual-level decision making. The dynamic and CGE model parameters are calibrated with historical data from U.S. Energy Information Administration (EIA), U.S. Department of Agriculture (USDA), U.S. Bureau of Economic Analysis (BEA), and U.S. Census, and scenario-specific future projections of energy consumption, GDP growth rates, and meat consumption. The land use model is estimated using the National Land Cover Database (NLCD) from the U.S. Geological Survey (USGS) in combination with economic, biophysical, and climate data from the U.S. Census, USDA, EIA, BEA, and other sources. The ensemble of different global conditions and corresponding macro-level economic and micro-level land use decisions are used as inputs to 5) an artificial intelligence-based regional watershed model, developed by training a random forest model with observed data and simulated outputs from the Soil and Water Assessment Tool (SWAT; G. Arnold et al., 2012), to evaluate regional water quality for the Maumee watershed, the largest watershed in the Lake Erie basin. The watershed model is calibrated using 2005-2015 streamflow data from USGS water stream gauge network and water quality data from the National Center for Water Quality Research (NCWQR) at Heidelberg University of Waterville gauge station located near the mouth of the Maumee River watershed in Toledo.

To explore the implications of global-to-local linkages for regional water quality policy targets, the calibrated model simulates five future scenarios distinguished by varying conditions of globalization and environmental stewardship from 2020 to 2050. These scenarios were developed in collaboration with a regional stakeholder advisory council drawn from professionals working in the agricultural, environmental and water sectors. Each scenario is associated with a Shared Socioeconomic Pathway (SSP) (Riahi et al., 2017) and a Representative Concentration Pathway (RCP) (Meinshausen et al., 2011) that are downscaled to the region. We use these downscaled values to project future population and climate change conditions for the Great Lakes region. In addition, each scenario is further characterized by a particular combination of global commodity prices, CO_2 prices, and sectoral productivity conditions over this same time period. Finally, we specify varying regional environmental stewardship conditions across scenarios by varying the trajecto-

ries of payments to landowners for agricultural land conservation enrollment and adoption rates for subsurface placement of fertilizer and filter strips. Scenario-specific climate projections for water quality assessment are based on Coupled Model Intercomparison Project phase 5 (CMIP5) Bias-Correction and Spatial Downscaling (BCSD). We assess water quality outcomes in terms of projected spring total phosphorus (TP) and spring dissolved reactive phosphorus (DRP) loads for the Maumee River watershed, considering nine combinations of climate conditions for RCPs corresponding to each scenario. We summarize these outcomes by decade to assess the likelihood that a 40 percent reduction in spring phosphorus is met nine of the ten years, which is the policy target set in 2012 by the Great Lakes Water Quality Agreement (GLWQA), a bi-national agreement between the U.S. and Canada.

Our results reveal that success in attaining the policy target is relatively uncertain, but that the uncertainty diminishes over time as BMP adoption rates increase across all scenarios. Given the range of conditions represented by the five scenarios, we find that only two of the scenarios are projected to attain the 40 percent spring DRP and TP reduction targets nine out of ten years by the 2030's and that none of them meet this target by 2025, which was the original timeline for meeting this target (USEPA, 2018). Both scenarios in which the decadal target is met in the 2030's have exceptionally high rates of best management practice (BMP) adoption, achieving 83 and 53 percent of total cropland acres with subsurface placement and buffer strips respectively by 2040. By comparison, the 40 percent reduction target is only met six (four) of the ten years for spring DRP (TP) in the 2030's for the two scenarios in which BMP adoption rates are the lowest. The results also reveal the importance of changing climatic conditions: one of the two scenarios in which the decadal target is met in the 2030's experiences higher than average precipitation in the 2040's. Despite adoption of subsurface placement and buffer strip rising to 90 and 63 percent respectively by 2050, the decadal target for TP is met eight, rather than nine, times in the 2040's under this scenario.

To further explore the relative effects of global and regional conditions on these outcomes, we compare land use and water quality outcomes across the five scenarios and the associated variations

in agricultural input and output prices, population trajectories, climate change, and land stewardship conditions. The results are consistent with the hypothesis that higher global commodity prices lead to increases in crop yields and cropland acres, although the latter result is conditional on the relative payments for land conservation enrollment. A sufficient level of conservation payments reduces the amount of land converted to working crop lands due to a greater number of acres enrolled in conservation. In terms of water quality outcomes, the results are less consistent. We find that the two scenarios with lower commodity prices and reduced cropland acres have better water quality outcomes and that this holds over most, but not all, scenarios and time periods. Surprisingly, we find that the two scenarios with greater intensification (i.e., higher cropland yields and rates of fertilizer application) are not associated with worse water quality outcomes, a result that may be driven by the relatively high adoption rates for subsurface placement that are reached in later years across both scenarios. Taken together, our results demonstrate the potential for local policies to ensure sufficient BMP levels that can act as a buffer to uncertain, changing global conditions. We conclude that this added insurance value of land stewardship policies should be considered in the design of efficient agricultural land conservation and BMPs. However, we have not yet quantified abatement costs nor incorporated BMP payments, and leave the assessment of efficient policies for future work.

This research contributes to the development of spatially detailed multi-sector, multi-scale IAMs—referred to as second generation IAMs (Fisher-Vanden and Weyant, 2020)— and the growing IAM literature on the food-energy-water (FEW) nexus (Kling et al., 2017) that systematically integrates global conditions, regional and state economic decisions, local land management practices, and hydrologic process in the analysis of regional water quality. These approaches are critical for understanding key interdependencies across scales, analyzing the trade-offs and the synergies among these resources (Biggs et al., 2015), capturing their impacts on ecological, physical, socio-economic, and political outcomes (Newell et al., 2019), and assessing local contributions towards the Sustainable Development Goals (SDGs) (Liu et al., 2018).

Many IAM-FEWS papers have examined linkages across FEW systems at national and global

scales. For example, Pastor et al. (2019) evaluate the impact of specific RCP and SSP scenarios on global land use, water consumption and food trade under water regulation policy scenarios. Van Vuuren et al. (2019) develop a set of model-based scenarios to analyze the future global dynamics of the FEW nexus under a baseline scenario of no policy response and compare projected global food and water trends with alternative response scenarios, including climate policies, higher agricultural yields, dietary change, and reduction of food waste. CGE models are a standard approach to representing global and regional trade flows and regional economic interactions and a number of CGE models have been built to study the roles of food, energy, trade, and policies (Pelikan et al., 2015; Marten et al., 2019). However, standard CGE models are often static, so recursive CGE models are often used to generate dynamics. In the literature of recursive CGE models, intertemporal decisions (e.g., investment and resource extraction) are often assumed to be exogenous or their associated policy functions are often assumed to be exogenously given with ad hoc simple equations. We improve this in our recursive CGE model by applying our dynamic regional forward-looking model's solution of intertemporal decisions for the Great Lakes region to generate the associated intertemporal decisions in each of five states in the region in a period-by-period manner.

Fewer studies have assessed global-to-local linkages in FEW systems. Notable exceptions include papers published in a 2023 special issue of *Environmental Research Letters* on global-to-local-to-global linkages of food-land-water systems (Hertel et al., 2023). For example, Liu et al. (2023) construct an integrated multi-scale framework for evaluating alternative nitrogen loss management policies for corn production in the U.S. by combining site- and practice-specific agro-ecosystem process models with a CGE model that embeds a grid-cell based analysis of the continental U.S. within a global economic model. However, a limitation of this and other studies is the static CGE framework and an assumption that the total amount of cropland is fixed over the projected time horizon. In assessing local and regional outcomes that are spatially dependent, including a range of ecosystem services, it is critical that spatially explicit, longer-term projections account for land use transitions that are observed at more disaggregate scales. The DRFEWS

framework considers a broader set of land use transitions, including transitions to/from cropland and pasture, wetlands, or forest, as well as irreversible transitions from cropland to urban. Our approach allows for the bottom-up, heterogeneous processes that drive Land Use Change (LUC) to determine shifts in land use over time while maintaining consistency with regional general equilibrium production and consumption during the simulation period (Prestele et al., 2017; Johnson et al., 2023). We predict county-level LUC, a computationally-light exercise, but measure LUC via aggregations of cell-level transitions. This provides us the ability to estimate models of specific transitions (e.g. cropland to urban use) as functions of local and regional determinants that can be updated over the course of the simulation (Verburg et al., 2019). Finally, this research also makes a novel contribution to hydrological modeling by developing an artificial intelligence (AI)-based regional watershed model that is much better suited for the repeated model runs that are necessary for scenarios. The SWAT has been used extensively for water quality management that addresses diverse sources of nutrients and sediment and mitigation actions for agricultural watershed (e.g., Hansen et al. 2021). However, it is time-consuming to calibrate and run, and further limited by the inability to change management practices over time during simulations. Our AI-SWAT model overcomes these challenges.

The rest of the paper is organized as follows. Section 2 provides a general overview of the coupled framework and scenarios to be examined using the framework. Section 3 describes the integration of all models and the details of each model and corresponding data. Sections 4, 5, and 6 explain the results of the economic model, land use model, and watershed model, respectively. Section 7 concludes the paper and presents future plans for improvement.

2 Coupled Framework and Scenario Development

The DRFEWS schematic diagram is displayed in Figure 1[1]. The framework first takes scenario-specific global and regional condition inputs. Second, based on these inputs, the economic[2] and land use models project the trajectories of key economic and land use outcomes through 2050 for each scenario. Third, outputs from these models feed into the regional watershed model for an ex-post evaluation of water quality.

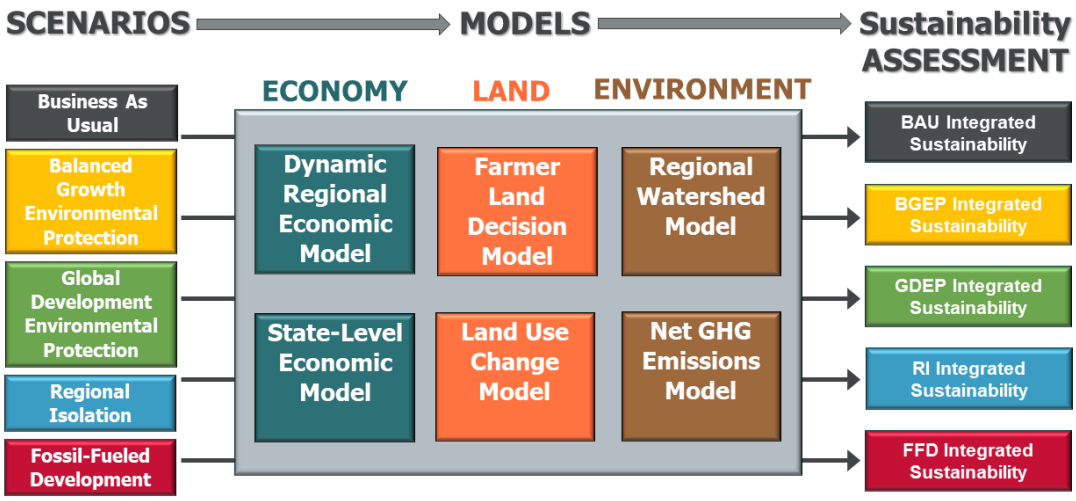

Figure 1: DRFEWS Coupled Framework

2.1 Scenario Development

Scenarios are useful for assessing outcomes when multiple sources of uncertainty and conditions of various interrelated components, including population, economic, climate, and other macro variables, must be represented in a consistent way. Unlike probabilistic modeling, a goal of scenarios is often to stress test less likely scenarios and to examine the range of outcomes that are plausible under varying, including more extreme, conditions. On this basis, we developed the following five

[1]The description of the sustainability assessment model is omitted in this paper to focus on the IAM and water quality assessment.

[2]The economic models are equipped with a greenhouse gas (GHG) emission module that computes GHG emissions by sector.

scenarios, associated with varying population, climate, economic, and environmental policy conditions at a global scale and varying land stewardship policies and practices at local and regional scales. The scenarios are tied to RCP and SSP combinations that are common in the literature and we adapt descriptions drawn from the SSP framework (O'Neill et al., 2020)[3]:

- **Business as Usual (BAU) (SSP2, RCP4.5)**: This pathway extrapolates the past and current global and regional conditions into the future. Regional population growth is moderate, growing steadily from 47.5 millions in 2020 to 56 millions by 2050. GHG emissions increase and then level off, reflecting moderate economic growth and subsequent technological changes that reduce emissions in later years. Markets also reflect middle of the road conditions in terms of trajectories of global commodity and carbon prices. Likewise, land stewardship conditions reflect moderate increases over time, including county-level Conservation Reserve Program (CRP) payments and BMP adoption rates that increase on average over time following a middle path.

- **Balanced Growth with Environmental Protection (BGEP) (SSP1, RCP2.6)**: This pathway describes an increasingly sustainable world in which global CO_2 prices are the highest and global GHG emissions reach net zero by around 2070. Global commodity markets reflect moderate price levels and global market integration and technological changes enable economic growth that is balanced by a sustainable use of resources. Regional population growth is moderate. Strong environmental stewardship policies and practices result in extremely high rates of conservation enrollments and BMP adoption.

- **Global Development with Environmental Protection (GDEP) (SSP4, RCP4.5)**: This pathway reflects fast-paced global development enabled by technological changes that offset rising emissions and are coupled with strong environmental preferences both globally and in the region. Global commodity markets reflect their highest price levels in this scenario. Because global growth is concentrated in the developing world, regional population growth

[3]More details of our scenario development are provided in a separate paper.

is moderate. Strong environmental stewardship policies and practices result in extremely high rates of conservation enrollments and BMP adoption.

- **Regional Isolation (RI) (SSP3, RCP6.0)**: Increased global disruptions and rising trade barriers slow the pace of globalization, leading to a stagnating regional population. Increased costs of global trade reduce global supply, leading to moderate increases in global commodity prices. Economic stagnation in the region results in less support for environmental protection and low levels of support for land stewardship.

- **Fossil-Fueled Development (FFD) (SSP5, RCP8.5)**: Global markets are increasingly integrated, leading to innovations and technological progress. Economic growth is based on an intensified exploitation of fossil fuel resources with the highest percentage of coal and natural gas uses. The lack of trade barriers and environmental regulations result in lower global commodity prices, high levels of GHG emissions, and low levels of support for land stewardship in the region. Greater globalization implies higher regional population growth.

Each scenario is specified with a distinct combination of global and regional projections, including the SSPs[4], RCPs[5], and national energy-related projections[6], all downscaled to the region. The projection alignment and scenario development are based on the inputs from our regional stakeholder advisory team and the relevant literature that aligns SSPs with RCPs (O'Neill et al., 2020). These downscaled values project population change, CO_2 prices, climate change conditions, and energy-related inputs for the region from 2020-2050 for each scenario. Each scenario is then further characterized by a particular combination of global commodity prices, sectoral productivity conditions, BMP adoption ratios, CRP enrollment payment over this same time period. These scenario-specific conditions are used by the corresponding models in the integrated framework to reflect the different global and regional conditions. Sections 4-6 present the details of global and

[4]International Institute for Applied Systems Analysis (IIASA) Shared Socioeconomic Pathways Scenario Database (SSP) https://iiasa.ac.at/models-tools-data/ssp

[5]IIASA RCP Database https://tntcat.iiasa.ac.at/RcpDb, and World Climate Research Programme (WCRP) https://wcrp-cmip.org/cmip-phase-5-cmip5

[6]U.S. Energy Information Administration, Annual Energy Outlook 2021

regional scenario-specific inputs used by each model, along with each model's results.

2.2 Hypotheses

In addition to examining the overall likelihood of attaining the GLWQA policy target under the range of global and regional conditions represented by these five scenarios, we aim to examine the following hypotheses that relate scenario assumptions to integrated model results:

H1. Increases (decreases) in global and/or regional demands for crops will (A) increase (decrease) the intensity of cropland use in the region (i.e., crop yields) and will (B) increase (decrease) total cropland acres.

H2. Increases (decreases) in cropland use at both the (A) intensive and (B) extensive margins will reduce (improve) water quality.

H3. Under high (low) land stewardship conditions, water quality outcomes are (not) invariant to changes in global or regional demands for agricultural commodities.

First, H1 is investigated in Section 4 by comparing the economic model results of crop yields and cropland acres from high and low global price scenarios. H2 and H3 are investigated in Section 6. To probe H2, given the identification from H1 of high or low cropland use results and corresponding scenarios, we compare those pairs of scenarios in terms of their water quality outcomes. Lastly, H3 can be analyzed with the comparison of water quality outcomes from a pair of two high (low) stewardship scenarios as they are specified with the same rates of best management practices, yet with differences in other conditions that are likely to impact water quality.

3 DRFEWS Model Integration

A key methodological innovation lies in the systemic integration of four sub-models. We formulate dynamic interactions between 1) a regional-level forward-looking dynamic economic model, 2) a state-level static computable general equilibrium (CGE) model, 3) a county-level land use

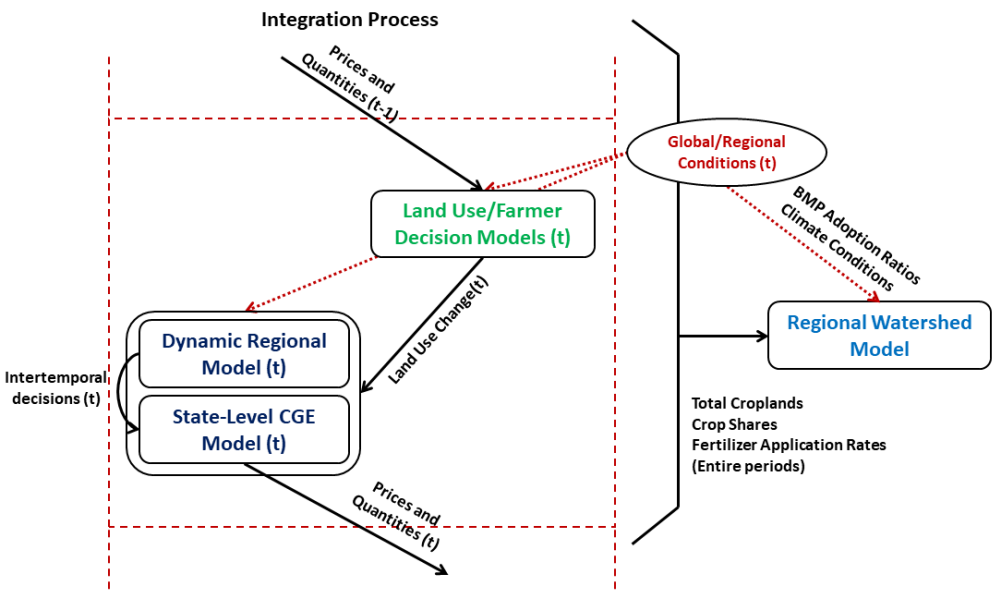

Figure 2: DRFEWS Integration Process

change model, and 4) a farmer's land management model. This enables a theoretically consistent integration from global conditions, to state-level economic decisions, and to local-level land use and individual-level land management decision making.

The schematic diagram of the integration is shown in Figure 2. First, at time t, the forward-looking dynamic regional economic model solves a dynamic regional welfare maximization problem with the starting period at t, given the exogenous scenario-specific time-varying global / national / regional conditions and the endogenous state vector $\mathbf{S}_t$ (the regional aggregate of state-level land, capital, labor, and resource stocks) at t. The solutions project a set of socially optimal investment and energy resource extraction decisions, along with production and consumption quantities, for each scenario. The derived intertemporal decisions (investment and extraction) at t, approximating general equilibrium solutions, are used as decisions rules in the state-level static CGE model at t, to make them together a recursive dynamic CGE model. We assume that each state makes investment and extract resources according to their shares of $\mathbf{S}_t$ within the region and the regional-scale manufacturing capital and electricity generation capacity investment and fossil fuel

extraction are allocated to each state proportionally (downscaling from regional intertemporal rules to state-level intertemporal rules).

Second, based on these intertemporal decisions and scenario-specific conditions, the five-state CGE model solves for the equilibrium prices and production, consumption, and trade quantities for each state at t. Among these economic outcomes, each crop's production and price, fertilizer use, state GDP, along with scenario inputs such as crop yield, fertilizer price, and state population, are used as inputs into the land use change model to determine the next period land allocation among five categories (cropland, pastureland, forest, wetland, and urban).

Third, the local-level land use allocation and land conservation program enrollment are projected by the county-level land use change model and the farmer's decision model. The outcomes are aggregated from a county-scale to a state-scale and region-scale, feeding back into the two economic models to compute $\mathbf{S}_{t+1}$. This provides available land at time $t+1$ for crop production, livestock production, and forest carbon sink. The iteration of these steps repeats until the year 2050 for each scenario to project the scenario-specific trajectories of economic and land use outcomes through 2050. This systemic integration enables an analysis of the effects of varying global conditions on local-level decision-making in a theoretically consistent framework.

After simulating the integrated economic and land use model, the ensemble of scenario inputs, such as global climate conditions and regional BMP adoption ratios, and corresponding macro-level economic (cropping shares and fertilizer application) and micro-level land use decisions (total working croplands and CRP enrollment) are used as inputs to the regional watershed model, AI-SWAT. AI-SWAT projects water quality indicators such as total and soluble phosphorus and total nitrogen loads in the Maumee River watershed in the Western Lake Erie Basin. The model also examines how frequently each scenario meets the 40% reduction target for the total and soluble phosphorus by 2050.

3.1 Economic Models

The DRFEWS economic model is formulated as a recursive dynamic CGE model, which solves for the regional- and state-level equilibrium prices and quantities through 2050. The recursive dynamic CGE model is comprised of a forward-looking dynamic regional economic model and a five-state static CGE model. This dynamic CGE model includes eight sectors for each of the five states in the region: farming (corn, soybean, wheat, specialty), livestock, food production, fossil fuel extraction (coal, natural gas), electricity generation (coal, natural gas[7], wind, solar), transportation energy services (gasoline, diesel, corn-base ethanol, electricity), general goods and services, and trading.

3.1.1 Data and Calibration

An extensive set of historical data between 2016 and 2021 and scenario-specific projections through 2050 are used to calibrate the model parameters and to simulate the model for each scenario. Agricultural data on row crops, specialty crops, and livestock production is primarily sourced from USDA National Agricultural Statistics Service (NASS). We use food processing, production, and consumption data from USDA Economic Research Service (ERS) yearbooks on food commodity use and processing. The state-level energy-related data on primary energy production and consumption and electricity generation and capacity are sourced from the U.S. EIA. State-level GDP and capital stock data come from the U.S. BEA. These historical data are used to specify the initial year (2016) endowment by state and also to calibrate both the regional-level and state-level economic models for all scenarios.

The model calibration process consists of three steps: 1) calibration of regional time-invariant parameters that are identical across the scenarios (e.g., elasticity of substitution in utility function, capital depreciation rate), 2) calibration of regional time-varying parameters for each scenario (e.g., total factor productivity by sector), and 3) calibration of state-level parameters that are identical

[7]There are two types of coal- and natural gas-fired power plants in the model: with and without 90% carbon capture and sequestration (CCS) technologies

across the scenarios (e.g., elasticity of substitution in production functions). The time-invariant parameters, universal across the scenarios, are mainly related to the historical and current characteristics of the economy for the region and states. Their calibration is conducted mainly using historical data, with a certain level of adjustment using the BAU scenario projections. On the other hand, regional-level parameters associated with intertemporal dynamics are distinct for each scenario and calibrated with respect to scenario-specific projections. These scenario projections include coal share of total fossil electricity generation, wind share of total renewable electricity generation, GDP growth rate, agricultural yield, and meat demand. The projections for each scenario are based on the downscaled projections from corresponding SSP and RCP scenario datasets and government agencies' projections (e.g., EIA Annual Energy Outlook), augmented by the discussion with regional stakeholder advisors to better reflect the reality of the region. By calibrating the economic model for each scenario, we are able to reflect the scenario-specific social, economic, climate trends in the model parameters.

3.1.2 Model Description

Figure 3 exhibits a simplified schematic diagram of a state economy in the five-state CGE model. Labor inputs used for the most sectors are omitted for simplicity. The figure shows only a single state economy whereas the actual model consists of five states in the region with an identical level of details for the economy and also accounts for domestic and international trade of commodities.

All economic agents in the economy optimize their decisions given the market and technological constraints. For example, in each state, the representative household maximizes their utility by their consumption choices of food, transportation energy, electricity, natural gas, and general goods, given their budget constraint. The budget constraint is constructed in a way that their incomes (profits from firms, land rents, capital rents, and wages) equal their expenses (consumption of goods and services, capital investment, and facility operation costs). The crop producers maximize their profits that equal the gross revenue from selling crops net of the costs of fertilizer, land, and labor inputs. By solving all optimization problems simultaneously subject to market clearing

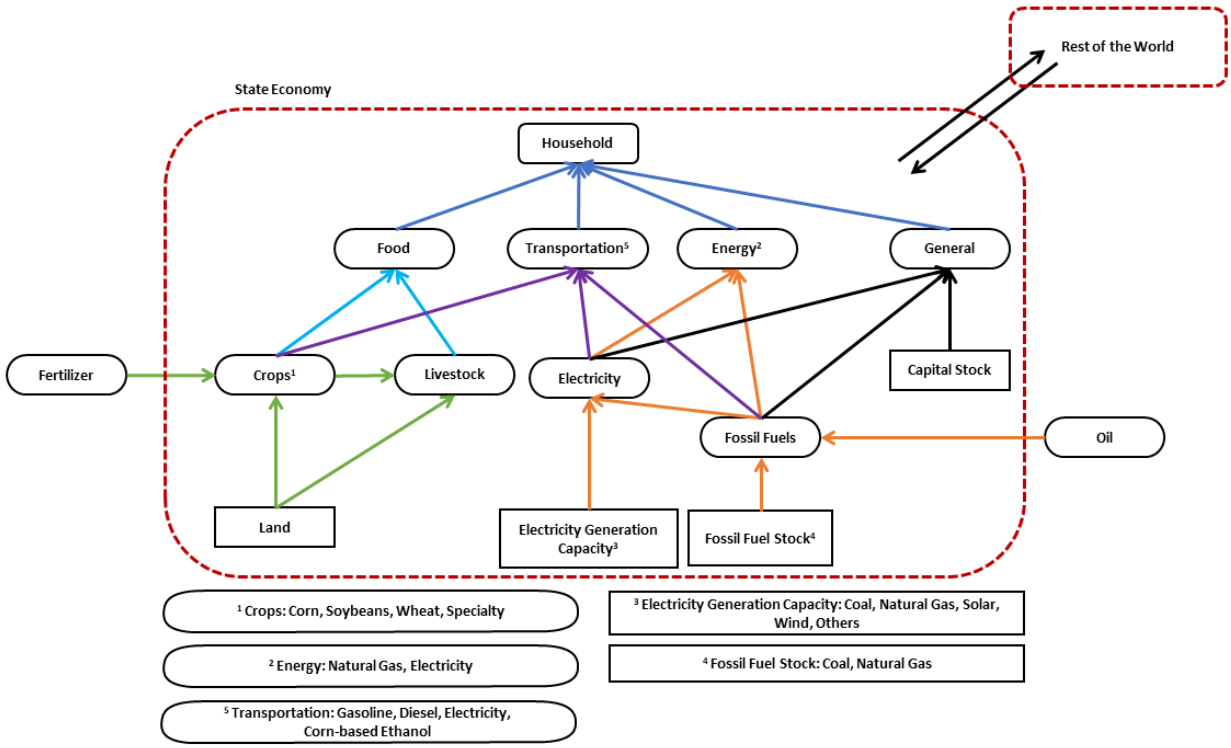

Figure 3: Economic Structure Schematic Diagram

conditions for each good, we identify a set of the equilibrium prices and quantities for every sector in every state given the period. All model equations and descriptions can be found in the Appendix A.

3.2 Land Use and Farmer Land Decision Models

We combine a variety of publicly available data describing regional land use, topography, soil quality, and economic activity at multiple scales to calibrate the land use and farmer management models. To measure LUC, we use 30m x 30m resolution remote-sensed data on land use/cover from the United States Geological Survey's (USGS) National Land Cover Database (NLCD) and aggregate cell-level changes over time to the county scale. We calculate the share of grid cells g in county i and LU j that transitions to LU k in each available period (e.g. 2001 to 2006, 2006-2011,

etc) where Ω_{gt} is the LU category for grid cell g at time t and G_i is the set of all grid cells included in county i.

$$Y_{ijkt} = \frac{\sum_g^{G_i} I(\Omega_{gt} = k, \Omega_{g(t-1)} = j)}{\sum_g^{G_i} I(\Omega_{g(t-1)} = j)} \tag{1}$$

This data is available for a set of years between 2001 and 2022, providing us with five snapshots of regional land use change over two decades. We estimate a collection of quasi-binomial logistic regression models that describe a set of feasible LU transitions (as measured by these LUC shares) as a function of average net returns to cropland in the county, population, GDP growth, previous LU, as well as time-invariant characteristics of land quality such as soil quality and slope[8]. We collect data on soil productivity and terrain from the Soil Survey Geographic Database (SSURGO), produced by the USDA National Resources Conservation Service (NRCS), along with agricultural data on crop production sourced from USDA NASS and economic data from the U.S. Census, the U.S. BEA and other sources. We choose time-varying characteristics, such as cropland net returns, that can be coupled with the economic models and updated over time in simulations (via updates in commodity prices, cropland rents, fertilizer use, and fertilizer prices). We allow for farmer-level heterogeneity in decisions to enroll in CRP; we treat this as a separate decision made on viable cropland and model farmer-level decisions to enroll land in conservation as a function of per-acre payments, county-level average cropland net returns, and other farmer-level characteristics. We use a choice experiment/survey developed for this project to estimate random effects models of conservation enrollment that separate the participation and quantity of enrollment decisions for farmers. We use the estimated models to simulate farmer-level conservation enrollment choices over time based on assumptions for CRP contract length and payments over time; in other words, for each farmer, we keep track of their accumulated stock of enrolled CRP land over time, allowing contracts to expire and renew over time based on simulated probabilities of participation and

[8]We collect all NLCD land cover tags into Cropland, Pasture/Grasslands, Forest, Wetlands, and Urban/Developed LU bins. Based on observed LUC for 2001-2021, we allow Cropland-Pasture, Cropland-Wetlands, Cropland-Urban, Pasture-Cropland, Pasture-Wetlands, Pasture-Urban, Pasture-Forest, Wetlands-Pasture, Wetlands-Cropland, Forest-Urban, and Forest-Pasture transitions. We exclude transitions that occur rarely in the sample period.

desired enrollment as predicted by our conservation enrollment models[9].

The land use and farmer land decision models, together determine county-level LUC in each time period given the scenario-specific global and regional conditions. Before simulating the projection, we draw the distribution of farmer characteristics (e.g., farm size and farmer age) for each county based on 2017 USDA Agricultural Census, and assign the baseline conservation practice adoption levels using a survey of farmers in the region. Within a simulation time-step, the LUC module downscales the state-level CGE model results and regional conditions to the county-level to obtain key variables including crop prices, fertilizer prices, GDP, fertilizer use, and crop mix. These variables are used to update land use and conservation enrollment predictors such as average net returns to cropland, county-level GDP growth, cropland rental rates, and pasture rental rates. Using the predicted rents together with physical factors describing each county as well as our scenario-dependent variables such as population, county-level LU transitions are predicted via the estimated regression models described above and LU shares are adjusted based on the predicted transition shares. The farmer management models project farmer-level changes to the conservation program enrollment. In the end, the aggregate county-level projections of land use and management practices to state-level and feed back to the economic models.

3.3 Regional Watershed Model

After the integrated economic and land use change model simulates projections through 2050 for all scenarios, the outcomes critical to water quality such as land use, crop rotations and fertilizer application rates are fed into the regional watershed model to predict impacts on water quality. Given the integrated model inputs, the farmer's BMP adoption ratios, and climate conditions for each scenario, the watershed model projects changes in water quality outcomes.

This watershed model, referred to as AI-SWAT, is developed using random forest regression, a

[9]More details on the integration steps and simulation will be included in future versions of the paper and can be provided upon request

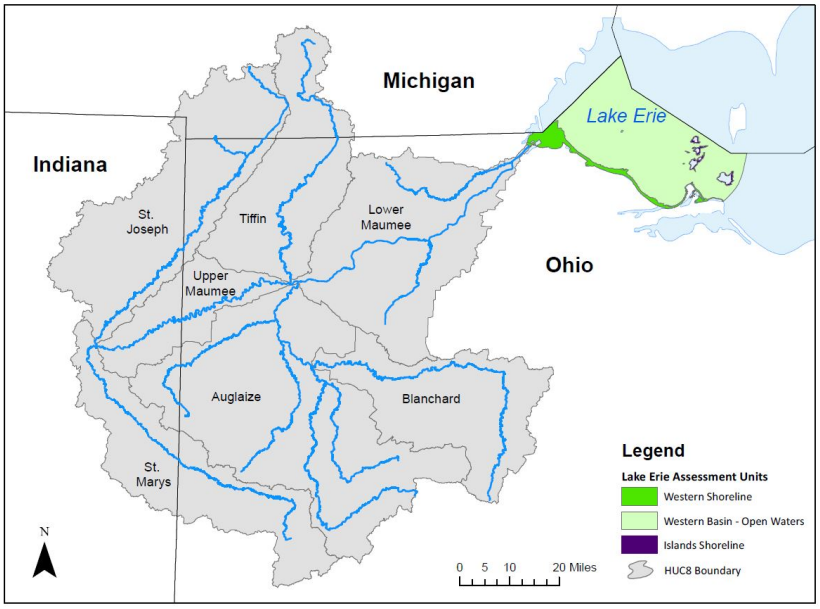

Figure 4: Maumee River Watershed (Source: Ohio EPA)

machine learning algorithm, and trained with observed data and outputs simulated from previous SWAT results Apostel et al. (2021). We developed this machine learning-based watershed model to be computationally efficient and easily integrable with other models (e.g., able to account for gradual changes in BMP adoptions), relative to the original process-based SWAT. The model is calibrated using 2005-2015 streamflow data from USGS water stream gauge network and water quality data from the NCWQR at Heidelberg University of Waterville gauge station (USGS gauge #04193500) located near the mouth of the Maumee River watershed in Toledo. Scenario-specific climate projections are based on CMIP5 BCSD. Three temperature models[10] and three precipitation models[11] are selected, considering the comprehensive model ranking specific to the Eastern Corn Belt Region (Wilson et al., 2022) and availability of projections for the RCPs corresponding to our scenarios. Thus, in total, nine combinations of temperature and precipitation projections are used as inputs for the watershed model.

This AI-SWAT model projects water quality outcomes, including streamflow, and loads of sediment, dissolved reactive phosphorus (P), total phosphorus, and total nitrogen (N), for each

[10] GFDL-ESM2G, NorESM1-M, MIROC5
[11] IPSL-CM5A-MR, MIROC-ESM-CHEM, MIROC5

scenario, in the Maumee River watershed in the Western Lake Erie Basin. In addition to those water quality indicators, the results examine how frequently this watershed will meet the 40% reduction target for the total and soluble phosphorus by 2050, which is the policy standard set in 2012 by the GLWQA.

3.4 Greenhouse Gases Emission by Sector

Greenhouse gases emissions are calculated using two life cycle assessment models, each based on the U.S. Environmentally-Extended Input-Output Models (USEEIO)[12] and the Greenhouse Gases, Regulated Emissions, and Energy Use in Transportation Model (GREET)[13]. These models calculate emissions factor, considering the full life cycle from the supply of raw material through the final production or disposal. The GHG emission factors derived for each sector are multiplied by the sectoral production to compute the gross emissions of the regional economy. The net emissions, then, are obtained by subtracting GHG sequestered by forest and carbon capture and sequestration technologies from the gross emissions. GHG emissions are expressed in terms of CO_2 equivalent unit, a measure used to compare various gases on the basis of their global warming potential. Emission factors for coal and gas electricity generation and general manufacturing and services sectors are time-varying to reflect the retirement of old, less efficient power plants and increased energy efficiency in manufacturing processes. All other sectors have constant coefficients.

4 Economic Model Scenario Inputs and Results

From Sections 4 through 6, figures are presented using the color code in Table 1 unless otherwise noted:

[12] https://www.epa.gov/land-research/us-environmentally-extended-input-output-useeio-models
[13] https://greet.es.anl.gov

Scenario		SSP	RCP	Color
Business as Usual	BAU	SSP2	RCP4.5	**Black**
Balanced Growth with Environmental Protection	BGEP	SSP1	RCP2.6	**Yellow**
Global Development with Environmental Protection	GDEP	SSP4	RCP4.5	**Green**
Regional Isolation	RI	SSP3	RCP6.0	**Blue**
Fossil-Fueled Development	FFD	SSP5	RCP8.5	**Red**

Table 1: Scenarios and Color Codes

4.1 Economic Model Scenario Inputs

This section presents a set of scenario inputs critical to the agricultural sector outcomes. First, our five-state region population projection is drawn from Jiang et al. (2020) which downscaled the SSP population projections to generate projections for the U.S. states [14]. The projections reflect the net effect of projected birth rates, death rates, and international and interregional migration. Population is a critical input that drives regional GDP, land use, and energy and food consumption. As described in Section 2.1, in the BAU scenario, the regional population is projected to moderately increase from 47.5 million in 2020 to 56 million in 2050. Two high stewardship scenarios (BGEP and GDEP) also project moderate increase in the regional population. The FFD scenario exhibits the highest population growth, whereas the RI scenario is the only non-increasing scenario.

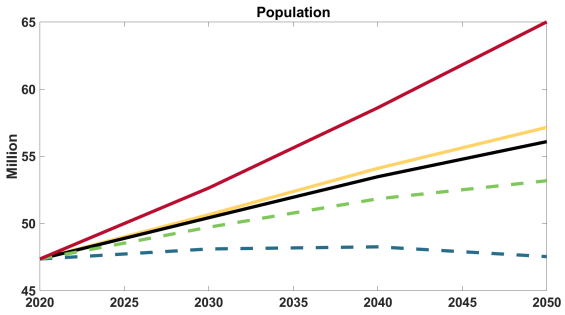

Figure 5: Population in the U.S. Great Lakes Region

[14]The International Institute for Applied Systems Analysis (IIASA) hosts the SSP scenario database, accessible via https://tntcat.iiasa.ac.at/SspDb. The underlying scientific data was published in Samir and Lutz (2017)

Global corn and soybeans prices are projected by economists in our research team in a way that reflect our best estimate of the global trends under different global economy and stewardship conditions. It needs to be noted that we project long-run average paths of agricultural commodity prices, rather than short-term prices that vary around the long-run average due to transitory global shocks. Specifically, we assume that in the BAU, corn and soybean prices remain stable at approximately 2020 levels ($4.2/bushel for corn, $10/bushel for soybeans). In general, compared to the BAU, scenarios with greater global market integration with limited trade barriers have lower commodity prices. Scenarios associated with strong level of environmental stewardship policies project higher prices. The net impacts of combining global market and stewardship conditions are presented in Figures 6-7: 50% higher in GDEP; 15% higher in BGEP; 20% higher in RI; 15% lower in FFD.

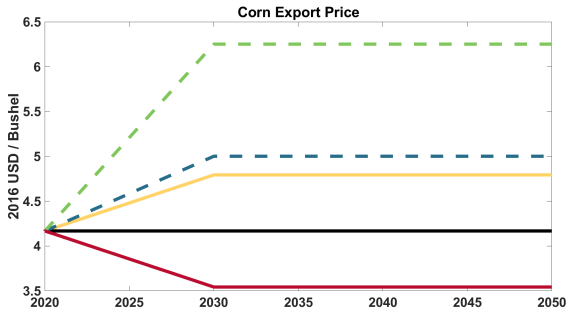

Figure 6: Corn Export Price

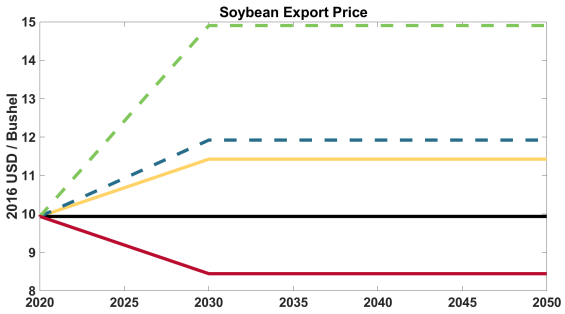

Figure 7: Soybean Export Price

The framework incorporates crop-specific fertilizer prices and their predicted trends, shown in Figure 8. The initial fertilizer prices are calculated using the nutrient price indices from the Federal Reserve Bank of St. Louis and the state-level average nutrient contents applied per acre for each crop provided by the USDA ERS. The price trend is predicted based on the statistical relationship, obtained from Schnitkey (2016), between historical fertilizer price changes and corn and natural gas prices. By using this relationship, the changes in corn prices and natural gas prices due to a carbon tax are reflected on the fertilizer prices by scenario.

Figure 9 shows scenario-specific conservation payments, a critical driver of farmers' decisions

to enroll in a conservation program in our land management model, and thus the size of working croplands. The BAU conservation payment rate growth (4.3%) is projected using historical rates of growth in actual CRP contract payments per acre between 2000-2019 in the region[15]. The variations across scenarios are determined through discussions with regional advisory stakeholders: for low stewardship scenarios (FFD and RI), we decrease the growth rate to 66% of the BAU; for high stewardship scenarios (BGEP and GDEP), we increase the growth rate by 50% of the BAU. The average conservation payment (in 2016 USD) in the region increases from $130/acre in 2020 to $250/acre, $160/acre, and $475/acre in 2050 in the BAU, low stewardship scenarios, and high stewardship scenarios, respectively.

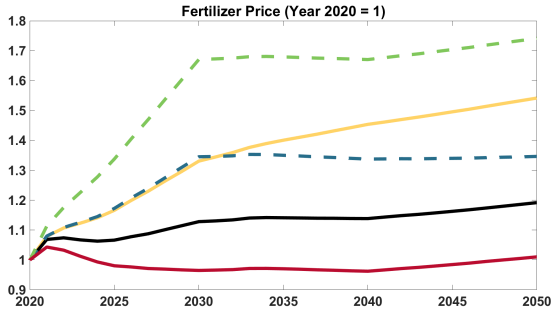

Figure 8: Fertilizer Price (Year 2020 =1)

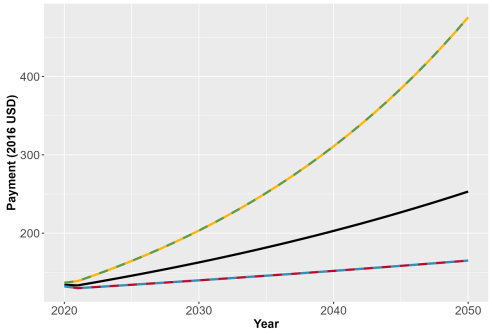

Figure 9: Conservation Payment

4.2 Economic Model Results

The economic model projects agricultural sector outputs, including cropland allocation, production, and fertilizer uses for corn and soybeans in the Great Lakes region for each scenario. The agricultural sector results showcase the projected responses of crop producers to the varied global environmental stewardship, climate, and market conditions and regional agricultural policies.

[15]See https://www.fsa.usda.gov/programs-and-services/conservation-programs/reports-and-statistics/conservation-reserve-program-statistics/index for details

4.2.1 Production and Land Allocation

Cropland and production projections for corn and soybean are exhibited in Figures 10-13. Total croplands available for production by county in each state are estimated by the land use change and the farmer's land management models. Then, the allocation of these total croplands to each crop production is projected by the dynamic CGE model.

As two main crops in the Great Lakes region, corn and soybean, in general, compete for land. In the BAU, soybeans are anticipated to be more profitable than corn over time; therefore, more land is projected to be used for soybean production. Total corn land and production decrease from 25 million acres and 4 billion bushels in 2020 to 3.5 billion bushels and in 2050, respectively. In contrast, total soybean land and production increase from 25 million acres and 1.4 billion bushels in 2020 to 32.5 million acres and 2.2 billion bushels, respectively. Of the two high stewardship scenarios, the BGEP favors soybean whereas the GDEP favors corn. This difference can be explained by commodity export prices (Figures 6 and 7), crop yields (Figures 14 and 15), and relative costs (e.g., fertilizer price, Figure 8), which together determine the crop's profitability. In the GDEP, with the highest expected agricultural commodity prices (50% higher than in the BAU), corn becomes more profitable than soybean. In the BGEP, the commodity prices are higher than in the BAU (15%), but the relative increase in fertilizer price is much higher (30% in 2050). As a fertilizer-intensive crop, corn production relies more substantially on fertilizer inputs than soybean production, and thus is more sensitive to fertilizer prices. The combined effects, insufficient to switch the order of the two crop's profitability, lead the BGEP corn and soybean lands closely to follow the trends of BAU until 2040 when two scenarios begin to deviate mainly due to the decreased total cropland in the BGEP.

The FFD is a scenario associated with the lowest agricultural productivity due to the worst global warming condition (RCP8.5) and the lowest commodity prices because of limited trade barriers and environmental regulations. With lower profitability, both corn and soybean exports reach zero towards the mid-century and are produced only to meet regional demand. Still, the pace of decrease in the FFD is modest because of higher population growth in this scenario. Unlike

soybean, corn land and production rebounds are observed after 2038, largely due to the steady use of corn for ethanol fuel production in the later years even after the export becomes zero. The RI scenario holds a set of favorable conditions for agricultural production—high productivity growth, high export prices, a relatively small increase in fertilizer cost—and all these together contribute to the increases in the allocated cropland and production of both crops.

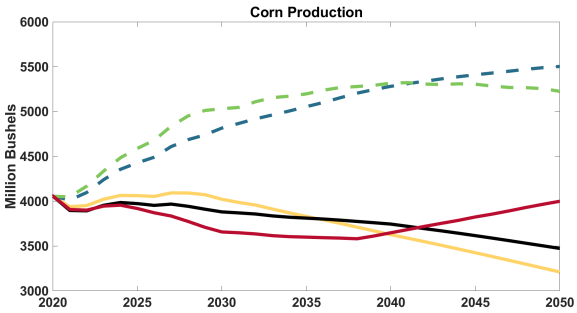

Figure 10: Corn Production

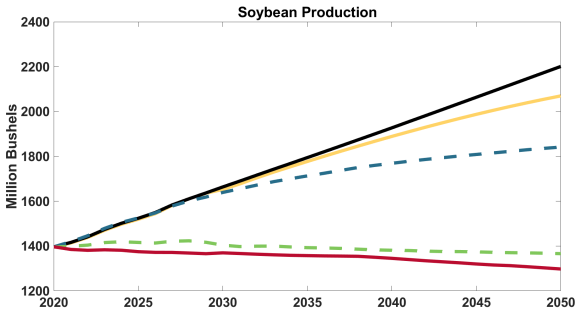

Figure 11: Soybean Production

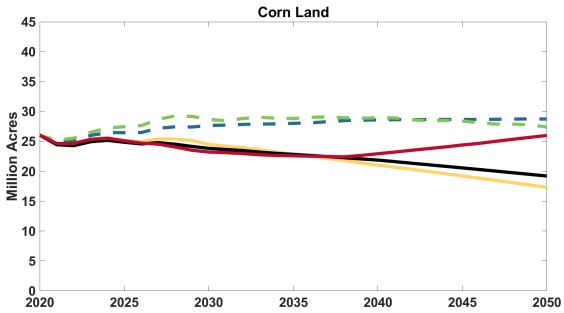

Figure 12: Corn Land

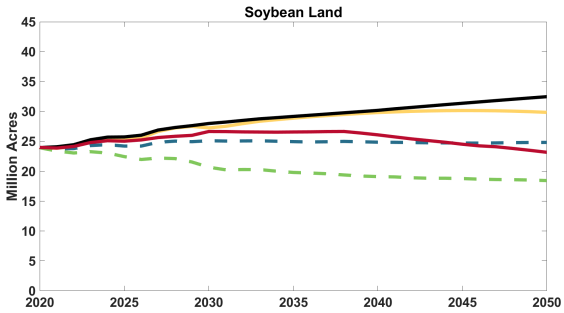

Figure 13: Soybean Land

4.2.2 Crop Yields

Figures 14 and 15 present corn and soybean yields, respectively, for each scenario. The BAU experiences yields generally increasing over time for both corn and soybeans, approximately by 15% through 2050, continuing current trends toward improvements in agricultural productivity. The yields are determined by scenario-specific assumptions, including climate conditions and technology advancement, along with fertilizer input quantity. Alternative scenarios mostly follow similar

patterns for both crops. In particular, the higher commodity price scenarios (GDEP and RI) show more substantial increases in cropland uses at intensive margins thanks to higher nutrient application rates (Figures 18-19) given higher profitability. Only the FFD observes a decrease in yields mainly driven by the worst climate conditions of RCP8.5.

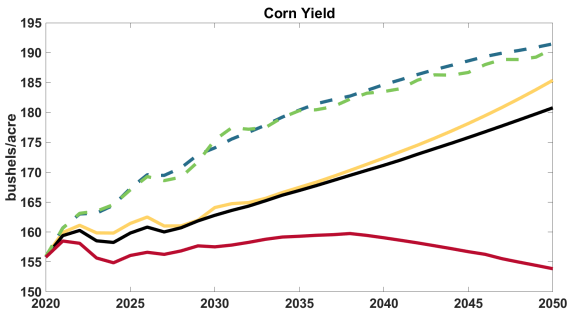

Figure 14: Corn Yield

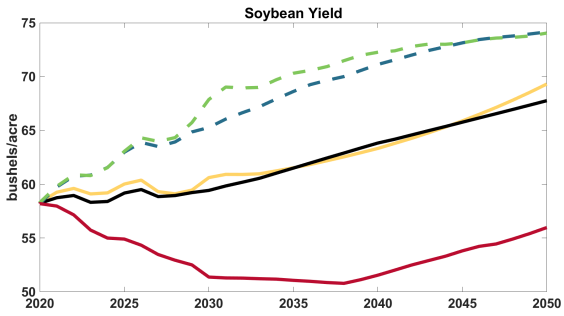

Figure 15: Soybean Yield

4.2.3 Total Croplands and Fertilizer Application

Total cropland in our integrated model remains roughly constant through 2050 under the BAU scenario (Figure 16). The two high stewardship scenarios (BGEP and GDEP) project the amount of the land used for crop production to decline compared to the BAU from roughly 52 million acres in 2020 to 49 million acres for BGEP and 47 million acres for GDEP in 2050. This is mainly explained by higher CRP payment rates that contribute to more enrollment in the CRP conservation program, estimated in land use models. Both low stewardship scenarios stay closer to the BAU trend than the high stewardship scenarios do.

By combining projections of acres planted to each crop and different rates of fertilizer application, the total amount of combined N, P and K fertilizers used for all crops (corn, soy, wheat, and specialty crops) in the region is projected. Figure 17 suggests that under the BAU scenario, the total application of fertilizers are projected to decline from 4.5 to 4.0 million short ton by 2050. In other scenarios, the total amount of fertilizer use varies over time. The higher commodity price scenarios (GDEP and RI) project the highest total fertilizer use, well above the BAU. The FFD scenario projects lower overall fertilizer use than the BAU until 2040, and then it also rises above the

BAU by 2050. The BGEP scenario tracks closely to the BAU until the early 2030s, then declines rapidly by 2050. The declines in total fertilizer use in the two high stewardship scenarios (GDEP and BGEP) after around 2035 can be explained by increasing fertilizer prices due to higher energy costs and decreasing total crop land in the region.

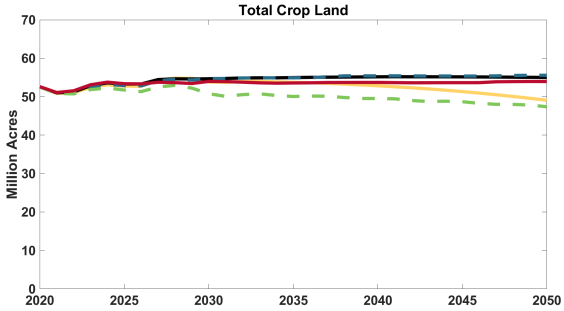

Figure 16: Total Croplands

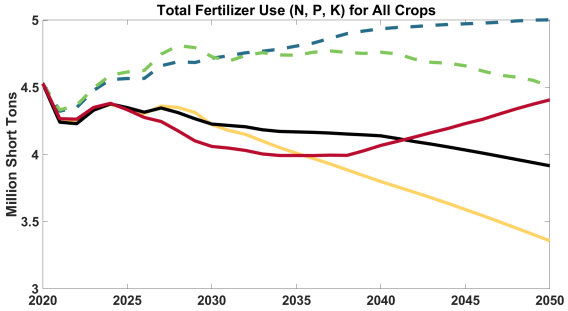

Figure 17: Total Fertilizer Use

The model assumes that per-acre fertilizer application rates are nearly constant over time, around 5% decline, in the BAU scenario (Figures 18 and 19). In other scenarios, the per-acre fertilizer application rates can be explained by the marginal return of the fertilizer, which is dependent on crop productivity and profitability. For instance, the GDEP, linked to higher productivity and higher profitability thanks to relative increase in crop price to cost, shows higher application rates. The FFD projects the lowest projected fertilizer application rates per acre. Fertilizer application rates are tied to per-acre yields, but will also play a role as an input to the water quality model results in Section 6.

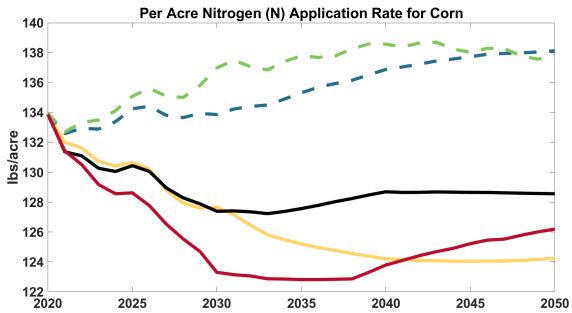

Figure 18: Per Acre Nitrogen (N) Application Rate for Corn

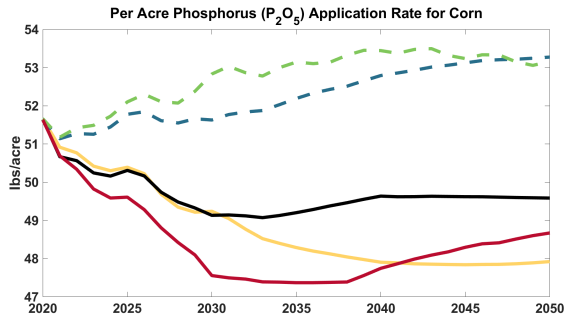

Figure 19: Per Acre Phosphorus (P_2O_5) Application Rate for Corn

4.2.4 Global Market Conditions and Regional Crop Production

In this subsection, we investigate the H1 hypotheses introduced in Section 2.2. Comparisons between a pair of scenarios with the same stewardship level confirm that our results are generally consistent with the H1. First, the effects of higher global commodity prices (H1A) are manifested as the increased crop yields (higher intensity of land use) under the GDEP and the RI, relative to the BGEP and the FFD, respectively (Figure 14 and 15). Second, the results partly support that higher prices lead to increased total cropland acres (H1B). Figure 16 shows that the RI maintains the greater acres of croplands than the FFD does. However, the two high stewardship scenarios are not consistent with the hypothesis, with the lower price scenario (BGEP) projecting the greater cropland acres than its higher price counterpart (GDEP). This result is mainly driven by the land conservation enrollment due to higher conservation payments in those scenarios (Figure 9). The last result implies that even when global market conditions stimulate an increase in total croplands and production, a sufficient amount of conservation payment still can lessen or prevent the conversion from idle lands to working croplands, potentially containing water quality degradation. Furthermore, the examination of H1 highlights the value of the integrated assessment framework that links global/regional conditions to state/local-level economic/land use decisions in assessing the environment, including water quality.

5 Land Use Model Results

Aggregated LUC predicted by each scenario are illustrated in Figures 20-24 below. In short, population and CRP enrollments constitute the two primary differentiating factors in LU between scenarios. Figure 22 illustrates that high stewardship scenarios break in trend from the other scenarios as CRP payments rise over time. Figures 25-29 illustrate the implications of these increasing CRP payments; for a subset of counties, particularly in Illinois and Indiana, payoffs for enrolling land in CRP become larger than the average net returns to cropping. We assume that CRP enrollments can be treated as grasslands made unavailable for grazing or other pasture uses; hence, high

stewardship scenarios contain more grasslands as time progresses as farmers enroll more of their cropland in CRP. Population projections are a key factor distinguishing between the GDEP and BGEP scenarios, placing pressures on LU conversion to urban use; conversion to developed/urban land use varies between scenarios by over 2 million acres for the region by 2050 (Figure 24). Our current forest models project little movement in aggregate forest land over time with all scenarios remaining near constant during the simulation period (Figure 23), but there are heterogeneous effects across counties in the region.

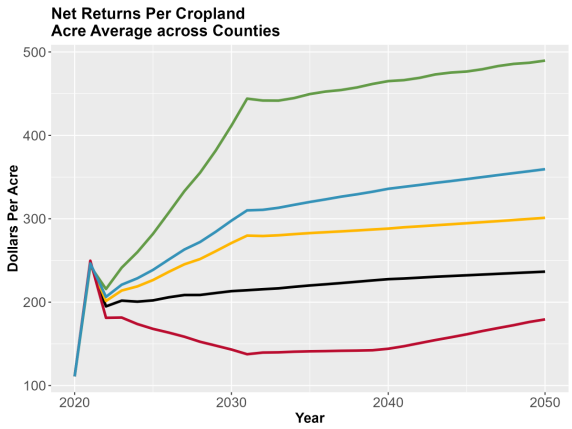

Figure 20: Net Returns Per Cropland Acre Average Across Counties

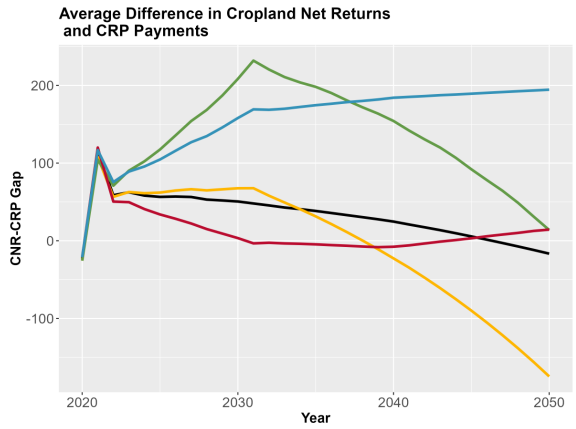

Figure 21: Average Difference in Cropland Net Returns and CRP Payments

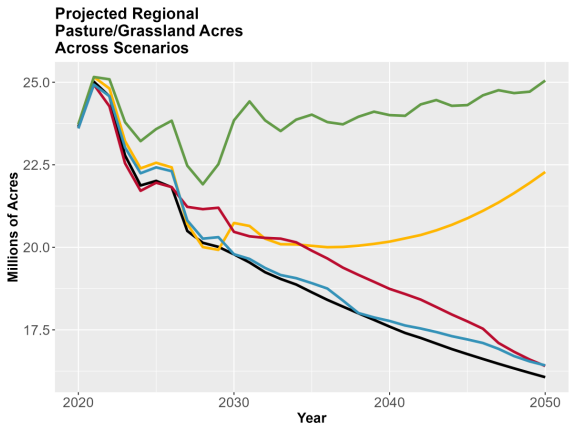

Figure 22: Projected Regional Pasture/Grassland Acres Across Scenarios

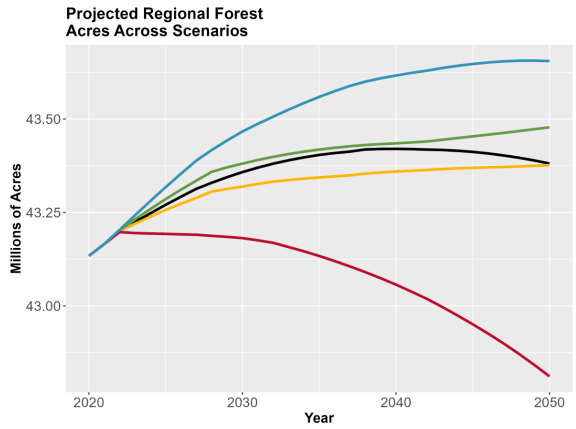

Figure 23: Projected Regional Forest Acres Across Scenarios

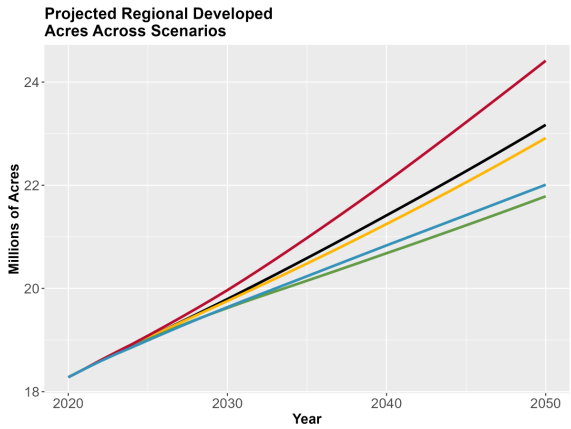

Figure 24: Projected Regional Developed Acres Across Scenarios

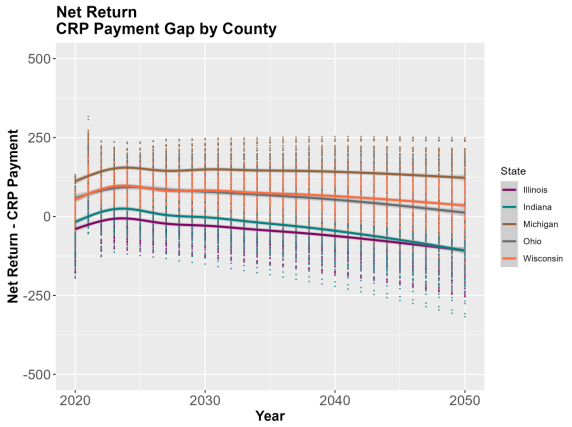

Figure 25: BAU Difference in Cropland Net Returns and CRP Payments by County

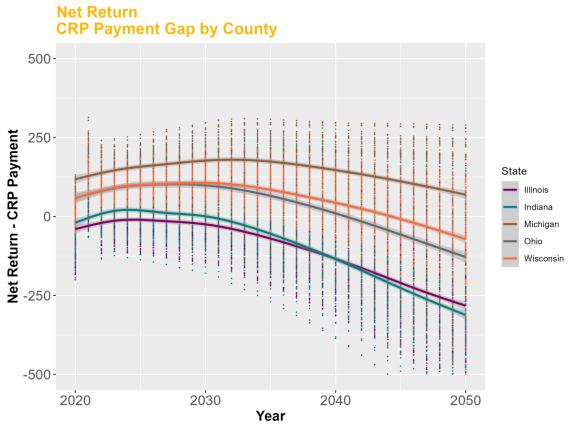

Figure 26: BGEP Difference in Cropland Net Returns and CRP Payments by County

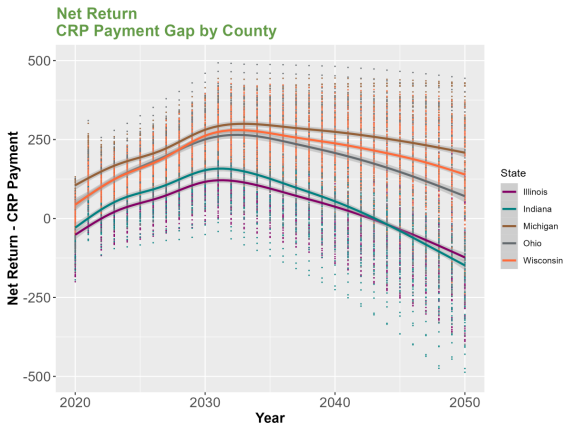

Figure 27: GDEP Difference in Cropland Net Returns and CRP Payments by County

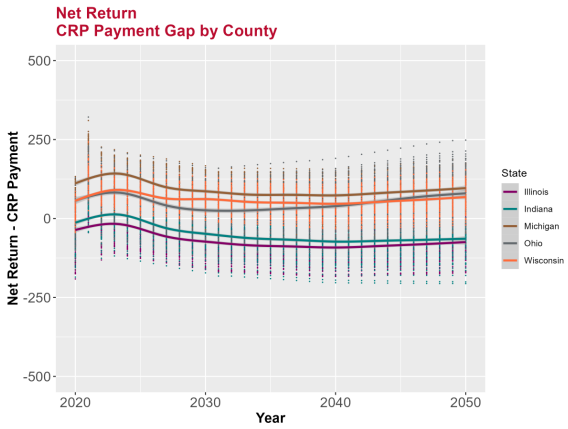

Figure 28: FFD Difference in Cropland Net Returns and CRP Payments by County

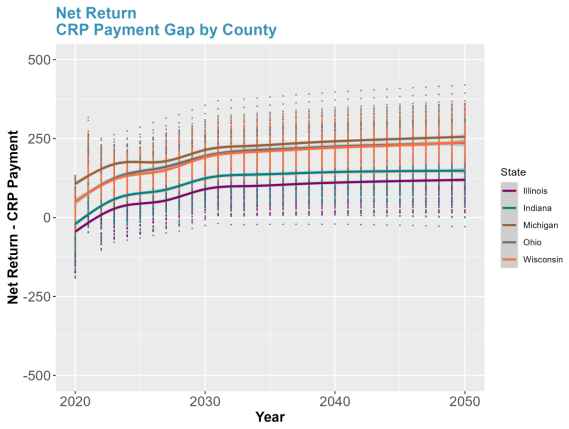

Figure 29: RI Difference in Cropland Net Returns and CRP Payments by County

6 Watershed Model Scenario Inputs and Results

In this section, we present scenario projections of water quality changes in the Maumee River watershed of northwest Ohio. These results are generated by a machine-learning-based model that is trained to simulate the outputs of a SWAT for the Maumee River watershed. The statistical model uses scenario-specific inputs on climate conditions, including precipitation and temperature, and rates of agricultural BMP adoption, along with results from the economic and land use models, such as projections of fertilizer application rates, crop rotations, and land use changes. In addition to changes in loads of nitrogen and phosphorus entering Lake Erie, we show how often this watershed will meet the 40% reduction target in frequency for total and soluble phosphorus, set for Lake Erie by the GLWQA in 2012.

6.1 Watershed Model Scenario Inputs

First, Figures 30-31 show climate conditions for different scenarios drawn from the nine combinations of global climate models simulated for corresponding RCPs. The temperature and precipitation are critical inputs into the regional watershed model as they impact sediment loading and water quality metrics (Kujawa et al., 2020). Under the BAU and the GDEP, both tied to the RCP4.5 climate projections, the annual temperature in the Maumee River watershed is expected to increase roughly 1 degree Celsius between 2020 and 2050. Both the BGEP and the RI, in general, show annual temperatures lower than the BAU, whereas the FFD, associated with RCP8.5 projections, observes over 1.5 degrees Celsius increase through 2050. The precipitation projections exhibit more variations across the scenarios. For example, the BAU (and GDEP) displays relatively gradual increase until 2040, followed by a decrease afterwards. The RI projects the precipitation increasing through 2030, and then decreasing to have the lowest among the scenarios.

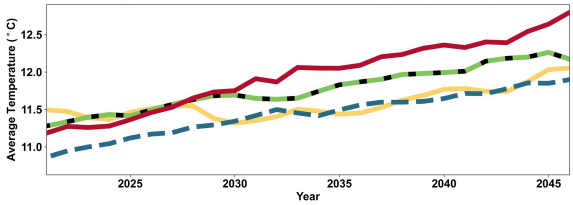

Figure 30: Annual Average Temperature of Maumee River Watershed, averaged across three climate models and rolling averaged for ten years

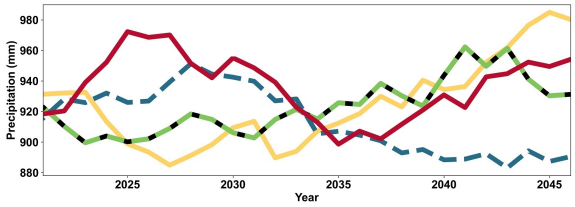

Figure 31: Annual Average Precipitation of Maumee River Watershed, averaged across three climate models and rolling averaged for ten years

Second, Figures 32-33 exhibit the projections of subsurface fertilizer placement and buffer strip adoption, respectively. The current percents of operators using subsurface placement of fertilizer and the annual rate of change under BAU are estimated using farmer surveys implemented at the state and regional level over the last 15 years (Kast et al., 2021; Burnett et al., 2018). Rates of change are adjusted up by 50% for high stewardship scenarios and down by 33% for low stewardship scenarios relative to rate of the BAU[16]. The current percent of cropland draining through a buffer are estimated by combining information from recent state and regional farmer surveys that report both the percent of operators using buffers and the percent of their cropland that drains through those buffers. Information from similar surveys over time are used to estimate the growth rate in each of these two components and to produce estimates of the BAU cropland protected by buffers into the future. The rates of change are adjusted up by 50% for high stewardship scenarios and down by 33% for lower stewardship scenarios relative to rate of the BAU[17].

[16] All growth rates are moderated after adoption approached 80% of farms to produce a flattened S-curve

[17] All rates are moderated after adoption approaches 50% of farms to produce a flattened S-curve

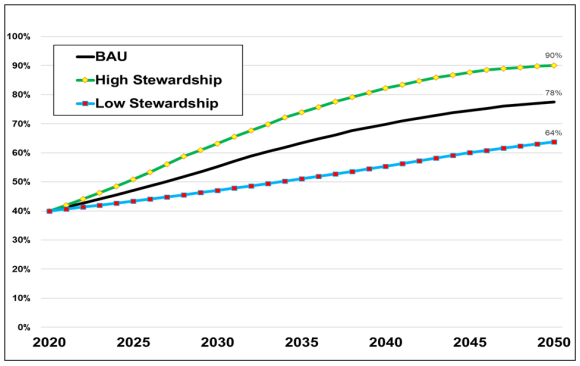

Figure 32: Percent Using Subsurface Fertilizer Placement

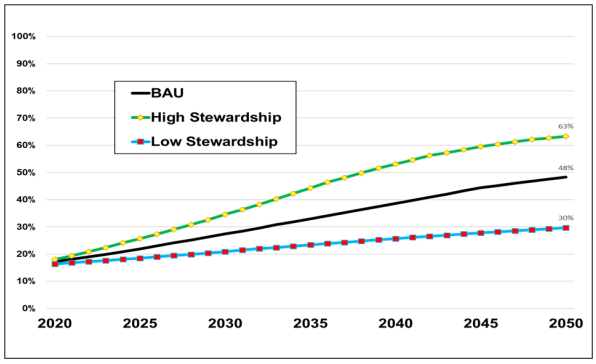

Figure 33: Percent of Regional Cropland Drained by Buffer

6.2 Watershed Model Results

Since the size and toxicity of algal blooms in Lake Erie are particularly linked to spring runoff during the months of March to July (Martin et al., 2021), we integrate information about temperature, rainfall, land use, crop rotations, and BMP adoption to project the level of spring[18] runoff at the mouth of the Maumee River for each scenario. The results in Figure 34 suggest that the BAU is expected to see slowly declining levels of spring runoff through 2050. Meanwhile, the two higher price scenarios (GDEP and RI) are projected to have higher levels of spring runoff in most years compared to the BAU. The GDEP is expected to exhibit persistently high spring runoff levels until the mid-2040s, followed by subsequent drops near the mid-century. Under the FFD scenario, there is a short spike in spring runoff in the mid-2020s, then a decline through the mid-century. Close to the mid-century, the BGEP ranks the first in terms of the streamflow amount, followed by the GDEP and the rest three scenarios (RI, FFD, and BAU).

One observation, from the comparison between the RI and FFD in the 2040s, is that the FFD, despite its higher precipitation, exhibits a similar streamflow with the RI. The trend can be attributed to the highest temperatures and evapotranspiration in the FFD, contributing to the lower runoff ratios.

A more notable result is the substantial difference in streamflow between the BAU and the

[18] Refers to March to July in the present paper.

GDEP, despite their common climate projections (RCP4.5). The difference signifies the advantage of the integrated assessment approach over a partial analysis in the water quality analysis. First, the two scenarios' distinct global market conditions lead to divergence in the agricultural sector in terms of a primary crop, fertilizer application rates, and yields, as shown in Section 4.2. This distinction results in the widening gap between two graphs through the middle of the period, before convergence takes place thanks to the GDEP's increased BMP adoption ratios, including the adoption of vegetative buffers, which are likely to reduce streamflow. Still, it requires a closer examination to isolate mechanisms behind the streamflow difference between the two scenarios, but the result hints the significance of global commodity market conditions as well as regional stewardship practices in water quality.

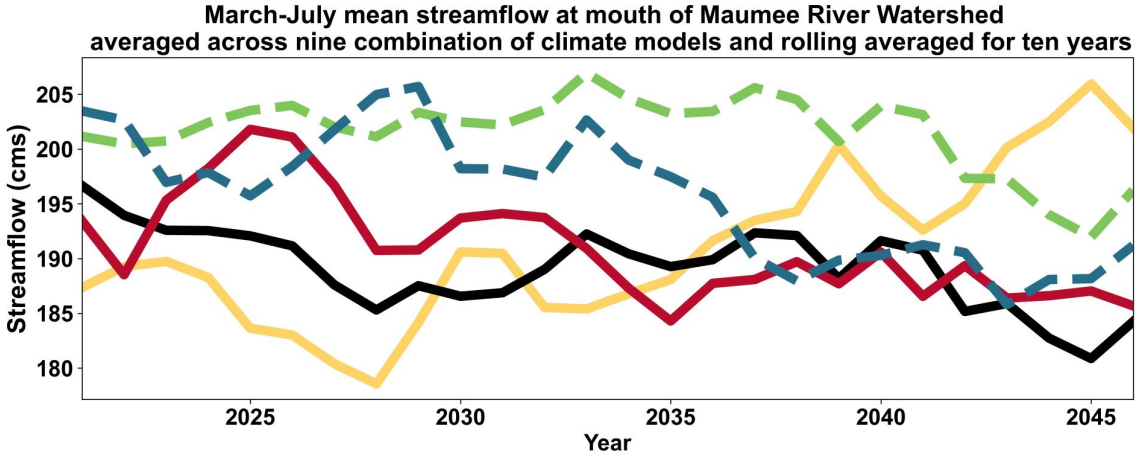

Figure 34: March-July Mean Streamflow at Mouth of Maumee River Watershed, Averaged across Nine Combination of Climate Models and Rolling Averaged for Ten Years

The Lake Erie Nutrient Reduction Agreement committed by the U.S. states and Canadian provinces to reduce the levels of total phosphorus (TP) and dissolved reactive or soluble phosphorus (DRP)[19] entering Lake Erie from their waters by 40%, particularly during the months of March-July (equivalent to 860 tons for TP and 180 tons for DRP, marked with gray solid lines in Figures 35 and 36, respectively). We use our watershed model to project TP and DRP loads from the Maumee River watershed during these critical spring months for each of our scenarios.

[19]Dissolved reactive phosphorus (DRP) and soluble phosphorus (SP) are used interchangeably in this paper as DRP is a subset of SP.

As annual projections fluctuate widely, we first focus on ten-year rolling averages to highlight the longer-term trends as in Baker et al. (2019).

TP loads between March and July under the BAU, starting at 1000 tons in 2020, are projected to reach the 40% reduction target by 2035, and further decline to roughly 750 tons by 2050. The two high stewardship scenarios (GDEP and BGEP) are projected to have even more rapid declines in spring TP loads from the Maumee River watershed. These scenarios reach the 40% reduction target by 2030 and 2026, respectively. Under both low stewardship scenarios (RI and FFD), projected spring TP loads are higher than BAU throughout the study period, and only approach the 40% reduction target by the mid-2040s.

DRP loads for March through July under the BAU are projected to decline from around 200 tons in 2020 to roughly 150 tons by 2050. The watershed reaches the 40% reduction target by 2025. The two high stewardship scenarios (GDEP and BGEP) are projected to see more rapid declines in spring DRP loads compared to the BAU over the entire study period. Under both low stewardship scenarios (RI and FFD), projected spring DRP loads are higher than the BAU throughout the study period, but achieve the 40% reduction target by the late-2020s.

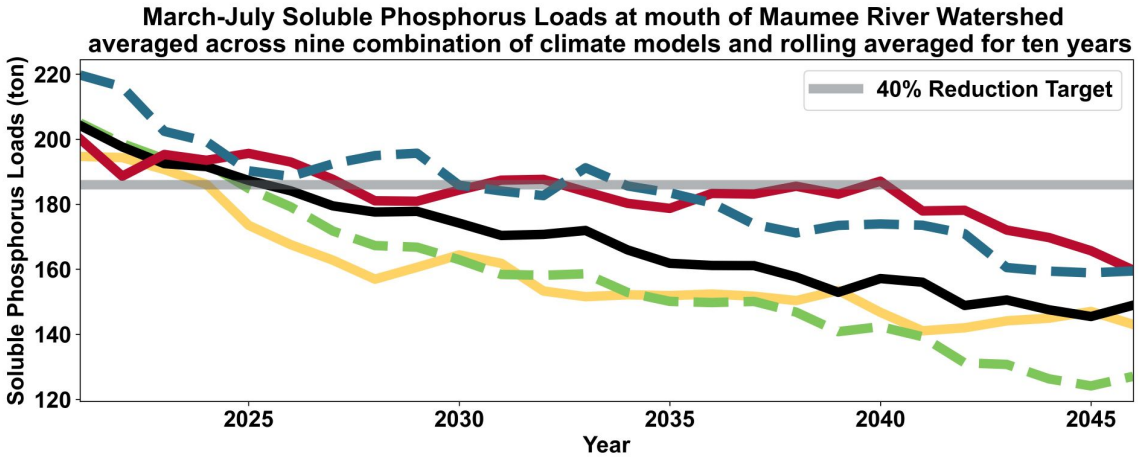

Figure 35: March-July Soluble Phosphorus Loads at Mouth of Maumee River Watershed, Averaged across Nine Combination of Climate Models and Rolling Averaged for Ten Years

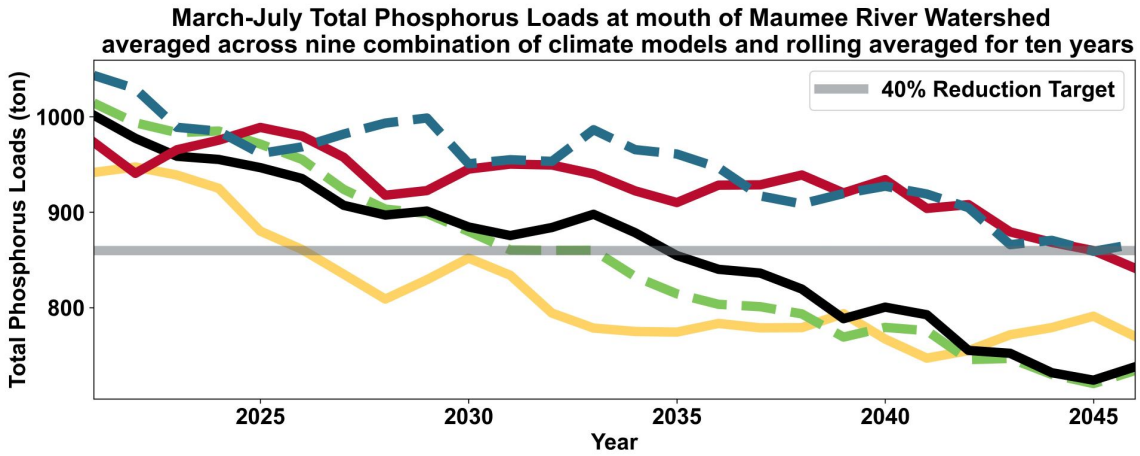

Figure 36: March-July Total Phosphorus Loads at Mouth of Maumee River Watershed, Averaged across Nine Combination of Climate Models and Rolling Averaged for Ten Years

As noted above, Ohio, Michigan, and Ontario have committed to reduce their spring total P and soluble P loads to Lake Erie by 40% (compared to 2008 levels) in nine out of ten years. Our model is able to examine the number of years in each decade that meet the 40% reduction target. Unlike the graphs above that illustrate a ten-year rolling average showing a long-term trend through the simulation period, Figures 37-38 provide an insight into the relative frequency with which the 40% target is met in a given decade under each scenario. In the figures, the gray diamond and the black bold line indicate the mean and median values of years meeting the 40% reduction target among those nine simulations for each scenario, respectively. The results suggest that the median values of the two high stewardship scenarios (BGEP and GDEP) generally tend to reach the 40% target for spring soluble P more frequently than the BAU's does in the 2020s and 2030s. By the 2040s, the GDEP scenario still outperforms the BAU, but the BGEP (eight of ten years) is slightly behind the BAU (nine of ten years). Under both low stewardship scenarios (RI and FFD), we project that the soluble and total P targets will be met less frequently than under the BAU in all three decades.

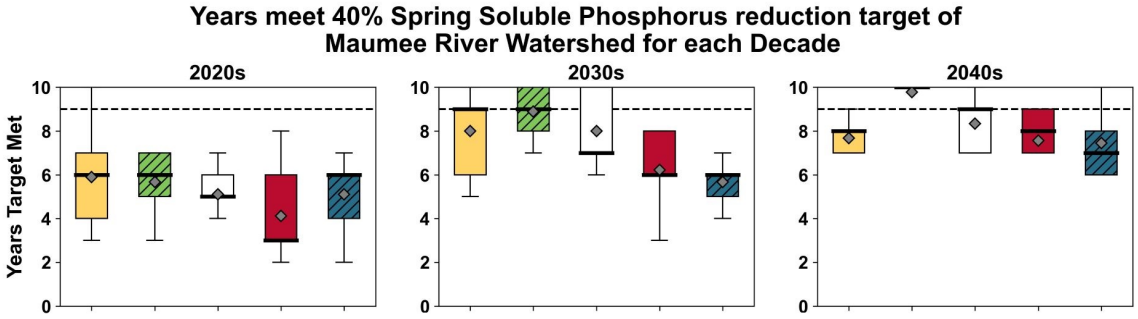

Figure 37: Years Meet 40% Spring Soluble Phosphorus Reduction Target of Maumee River Watershed for Each Decade

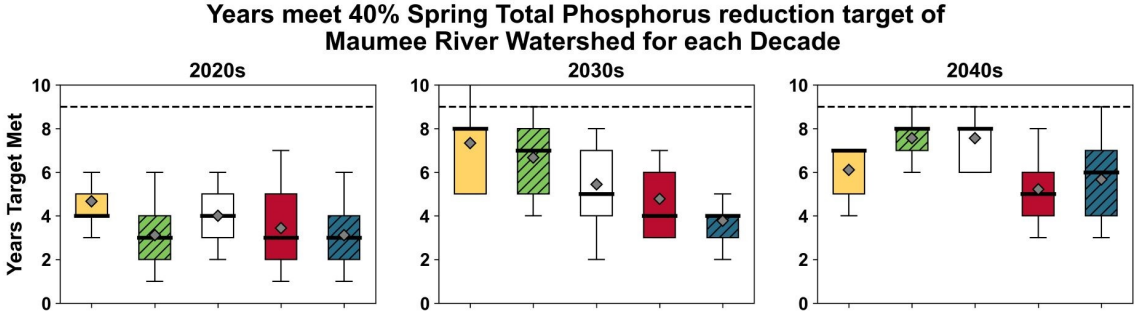

Figure 38: Years Meet 40% Spring Total Phosphorus Reduction Target of Maumee River Watershed for Each Decade

6.2.1 Integrated Framework-Based Water Quality Analysis

This section interprets the water quality results in the context of the integrated framework and also examines the two remaining hypotheses, H2 and H3, introduced in Section 2.2. First, while the rolling-averaged DRP and TP results in Figures 35 and 36 show the effectiveness of BMP adoption in all scenarios, the results in Figures 37 and 38 illustrate that success in the earlier years in attaining the policy target is relatively uncertain and highly dependent on economic, environmental, and policy conditions. Given the range of conditions represented by the five scenarios, we find that only two of the scenarios are projected to attain the 40 percent spring DRP and TP reduction targets nine out of ten years by the 2030's and that none of them meet this target by 2025, which was

the original timeline for meeting this target (USEPA, 2018). Both the GDEP and BGEP scenarios in which the decadal target is met in the 2030's have exceptionally high rates of BMP adoption, achieving 83 and 53 percent of total cropland acres with subsurface placement and buffer strips respectively by 2040. By comparison, the 40 percent reduction target is only met six (four) of the ten years for spring DRP (TP) in the 2030's for the two scenarios in which BMP adoption rates are the lowest.

The results also reveal the importance of changing climatic conditions and agricultural activities. The BGEP shows the most dynamic trend: it experiences relatively larger fluctuations around 2030 and, more notably, slower declining rates in the 2040s despite its highest BMP adoption ratios and smaller working croplands in the corresponding period. The variations in the earlier years coincide with its volatility in precipitation and streamflow in those years. Furthermore, the reduced declining rates in the 2040s align with higher precipitation and streamflow in that period.

The comparison between the two low stewardship scenarios provides another insight. These scenarios exhibit very similar trends in both DRP and TP loads despite their significant difference in agricultural intensity: the RI is characterized with the greatest croplands, fertilizer application, etc. The trend may be partially explained by their similar amount of streamflow and identical projections of BMP adoption ratios. Taken together, these results suggest that BMPs play a significant role in reducing DRP and TP, but at the same time, the changes in precipitation can compromise the effectiveness of the practices, as shown in the literature (Bosch et al., 2014; Kujawa et al., 2022).

To examine each of the hypotheses, we compare the results across scenarios to assess whether they are consistent with the hypothesized relationships. H2 hypothesizes the relationship between water quality and variations in cropland uses at (A) intensive margins and (B) extensive margins. The scenario results are inconsistent with H2A: although both GDEP and RI have higher crop yields with higher rate of fertilizer application, and in addition RI has a lower streamflow, DRP and TP loads are lower under GDEP than RI. This might suggest that the increase in cropland use at the intensive margin alone does not always lead to the deterioration of water quality. This statement is partly supported by the insubstantial differences in water quality between the highest-

yield scenario, RI and the lowest-yield scenario, FFD. We find greater consistency in the scenario results with H2B. The scenarios with fewer cropland acres (GDEP and BGEP) perform better in terms of water quality indicators than those with relatively constant or slightly increasing amount of croplands (FFD and RI). However, despite its smaller working croplands, the BGEP exhibits similar or worse water quality in the 2040s than the BAU. As explained above, the illustrates the offsetting effects from precipitation, which increases in the 2040's under this scenario.

Lastly, the results are largely consistent with H3. Both the BGEP and GDEP scenarios have the identical BMP adoption ratios, but differ in their global and regional economic conditions. Throughout the 2020's and 2030's, the two scenarios exhibit similar levels of TP and DRP loads, diverging only in the 2040's when precipitation increases under the BGEP scenario. The increased precipitation imposes a negative impact on water quality in the BGEP scenario. Nevertheless, the impact is rather moderate, likely due to its higher BMP ratios. Likewise, the RI and FFD scenarios have equal levels of BMP adoption, but differ in other conditions. The RI is the most agriculturally-intensive scenario with the greatest cropland acres, yields, and fertilizer uses whereas the FFD is characterized with relatively lower intensity in agricultural activities. However, their water quality results are nearly identical throughout the simulation period. Their identically increasing BMP adoption ratios, together with relatively moderate climate conditions, would contribute to this trend, mitigating the influences from the regional economy and global market. These results are also supported by the decadal assessment (Figures 37 and 38) that shows that, despite confounding factors, increasing rates of BMP adoption across all scenarios leads to more frequent attainment of targeted DRP and TP reductions.

7 Conclusion and Future Plans

The research introduces an integrated assessment framework of food, energy, and water systems to assess the impacts of changing global economic/climate and regional stewardship conditions on the regional economy and environmental quality. By systematically integrating multiple sub-models

that account for regional- and state-level economic decisions, county-level land use transitions, and farmer-level land conservation decisions, along with global conditions, the study develops a theoretically consistent framework of examining decision making across scales and assessing global-to-local interactions.

The dynamic CGE model has multiple advantages in the context of IAM. First, thanks to the fully-dynamic integration with the land use model, our model is capable of solving for equilibrium quantities and prices given updated total available croplands for each state economy every period. Instead of using ad hoc intertermporal decisions rules, often used in standard recursive dynamic CGE models, we build a separate forward-looking dynamic model that determines the optimal intertemporal decisions on investment and resource extraction. Moreover, as we calibrate the dynamic model for each scenario, our model parameters is able to reflect the social, economic, and climate conditions of each scenario, thus contributing a logically consistent modeling to our scenarios framework.

We calibrate and integrate a county-level LUC model that measures cell-level transitions between specific land uses which takes into account local land heterogeneity and is coupled with regional and global economic factors; this global/regional to local linkage allows for LU to change in response to shifts in higher-scale factors. We then aggregate this LUC up to the state-level, linking the bottom-up LUC process with regional economic systems. In addition, we make use of a choice experiment conducted by a sample of regional farmers to estimate a two-step model of conservation land enrollment; this allows us to take into account farmer-level heterogeneity in their likelihood to participate in CRP as well as their scale of enrollment. By keeping track of enrollment at the scale of simulated farmers across the region, we simulate how changes in CRP payments affect enrollment decisions differently over space and time, incorporating key farmer-level and spatial heterogeneities that determine aggregate conservation enrollment and subsequent water quality changes.

The AI-SWAT model is an important computational innovation. Despite its extensive use for water quality assessment, the SWAT might not be suitable for scenarios framework that requires

repeated runs by scenario and integrability with other models. The AI-SWAT model is computationally efficient. In addition, trained with the observed data and SWAT simulated results for future farming management scenarios, our watershed model is capable of predicting the water quality outcomes for each future scenario, adaptively taking into account changing inputs from economic and land use models and regional land stewardship conditions, including BMP adoption rates.

Despite these multiple contributions to advancing regional dynamics IAMs, the analysis of our water quality results is still preliminary. The principle advantage of a scenarios framework—that multiple uncertainties can be considered jointly by bundling a range of specified conditions into a single scenario—also makes it challenging to interpret the results in a systematic cause-and-effect manner. Doing so requires additional model simulations to identify and quantify the extent to which any single factor drives a particular result and to what extent. For example, to further investigate whether BMP adoption plays the most critical role in determining water quality across the scenarios, we would need to simulate each scenario many times by systematically varying combinations of global market and climate conditions and conservation program payments, etc. This test would provide implications for policy effectiveness and robust policies across scenarios. We plan to conduct additional model simulations to better assess the relative effects of global versus local conditions. With more modeled outputs, we also plan to use statistical analyses or machine learning interpretation methods, such as SHapley Additive exPlanations (SHAP) (Lundberg and Lee, 2017), to identify and compare each variable's contribution to water quality outcomes. In addition, we plan to incorporate payments for BMPs and use modeled outputs to project the marginal abatement costs of water pollution for different land use and management practices. For instance, with varying levels of conservation program payments, we can investigate farmers' responses to the policy changes and decisions on land conservation, ultimately affecting the regional water quality. The analysis would allow us to examine the effectiveness of the government payments in reducing water pollution and the robustness of different policies to the variations in global and regional conditions reflected across scenarios. Lastly, we are currently working on a more granular-scale land use model to tightly couple heterogeneous farmer management decisions and biophysical model

outputs to allow for more robust analysis of biophysical outcomes and policy effectiveness.

References

Anna Apostel, Margaret Kalcic, Awoke Dagnew, Grey Evenson, Jeffrey Kast, Kevin King, Jay Martin, Rebecca Logsdon Muenich, and Donald Scavia. Simulating internal watershed processes using multiple SWAT models. *Science of the Total Environment*, 759:143920, 2021. ISBN: 0048-9697 Publisher: Elsevier.

David B. Baker, Laura T. Johnson, Remegio B. Confesor, John P. Crumrine, Tian Guo, and Nathan F. Manning. Needed: Early-term adjustments for Lake Erie phosphorus target loads to address western basin cyanobacterial blooms. *Journal of Great Lakes Research*, 45(2): 203–211, 2019. ISSN 0380-1330. doi: https://doi.org/10.1016/j.jglr.2019.01.011. URL `https://www.sciencedirect.com/science/article/pii/S0380133019300310`.

Eloise M. Biggs, Eleanor Bruce, Bryan Boruff, John M. A. Duncan, Julia Horsley, Natasha Pauli, Kellie McNeill, Andreas Neef, Floris Van Ogtrop, Jayne Curnow, Billy Haworth, Stephanie Duce, and Yukihiro Imanari. Sustainable development and the water-energy-food nexus: A perspective on livelihoods. *Environmental Science & Policy*, 54:389–397, 2015.

Nathan S. Bosch, Mary Anne Evans, Donald Scavia, and J. David Allan. Interacting effects of climate change and agricultural BMPs on nutrient runoff entering Lake Erie. *Journal of Great Lakes Research*, 40(3):581–589, 2014. ISSN 0380-1330. doi: https://doi.org/10.1016/j.jglr.2014.04.011. URL `https://www.sciencedirect.com/science/article/pii/S038013301400094X`.

E. Burnett, R. S. Wilson, A. Heeren, and J. Martin. Farmer adoption of cover crops in the western Lake Erie basin. *Journal of Soil and Water Conservation*, 73(2):143–155, 2018. ISBN: 0022-4561 Publisher: Soil and Water Conservation Society.

Karen Fisher-Vanden and John Weyant. The Evolution of Integrated Assessment: Developing the Next Generation of Use-Inspired Integrated Assessment Tools. *Annual Review of Resource Economics*, 12(1):471–487, 2020.

J. G. Arnold, D. N. Moriasi, P. W. Gassman, K. C. Abbaspour, M. J. White, R. Srinivasan, C. Santhi, R. D. Harmel, A. van Griensven, M. W. Van Liew, N. Kannan, and M. K. Jha. SWAT: Model Use, Calibration, and Validation. *Transactions of the ASABE*, 55(4):1491–1508, 2012.

Amy T. Hansen, Todd Campbell, Se Jong Cho, Jonathan A. Czuba, Brent J. Dalzell, Christine L. Dolph, Peter L. Hawthorne, Sergey Rabotyagov, Zhengxin Lang, Karthik Kumarasamy, Patrick Belmont, Jacques C. Finlay, Efi Foufoula-Georgiou, Karen B. Gran, Catherine L. Kling, and Peter Wilcock. Integrated assessment modeling reveals near-channel management as cost-effective to improve water quality in agricultural watersheds. *Proceedings of the National Academy of Sciences*, 118(28):e2024912118, 2021.

Thomas W. Hertel, Elena Irwin, Stephen Polasky, and Navin Ramankutty. Focus on global–local–global analysis of sustainability. *Environmental Research Letters*, 18(10):100201, 2023. ISBN: 1748-9326 Publisher: IOP Publishing.

Leiwen Jiang, Brian C. O'Neill, Hamidreza Zoraghein, and Steve Dahlke. Population scenarios for US states consistent with shared socioeconomic pathways. *Environmental Research Letters*, 15(9):094097, 2020. ISBN: 1748-9326 Publisher: IOP Publishing.

Justin Andrew Johnson, Molly E. Brown, Erwin Corong, Jan Philipp Dietrich, Roslyn C. Henry, Patrick José von Jeetze, David Leclère, Alexander Popp, Sumil K. Thakrar, and David R. Williams. The meso scale as a frontier in interdisciplinary modeling of sustainability from local to global scales. *Environmental Research Letters*, 18(2):025007, February 2023. ISSN 1748-9326. doi: 10.1088/1748-9326/acb503. URL `https://dx.doi.org/10.1088/1748-9326/acb503`. Publisher: IOP Publishing.

Jeffrey B. Kast, Margaret Kalcic, Robyn Wilson, Douglas Jackson-Smith, Nicholas Breyfogle, and

Jay Martin. Evaluating the efficacy of targeting options for conservation practice adoption on watershed-scale phosphorus reductions. *Water Research*, 201:117375, 2021. ISBN: 0043-1354 Publisher: Elsevier.

Catherine L. Kling, Raymond W. Arritt, Gray Calhoun, and David A. Keiser. Integrated Assessment Models of the Food, Energy, and Water Nexus: A Review and an Outline of Research Needs. *Annual Review of Resource Economics*, 9(1):143–163, 2017.

Haley Kujawa, Margaret Kalcic, Jay Martin, Noel Aloysius, Anna Apostel, Jeffrey Kast, Asmita Murumkar, Grey Evenson, Richard Becker, and Chelsie Boles. The hydrologic model as a source of nutrient loading uncertainty in a future climate. *Science of The Total Environment*, 724:138004, 2020. ISBN: 0048-9697 Publisher: Elsevier.

Haley Kujawa, Margaret Kalcic, Jay Martin, Anna Apostel, Jeffrey Kast, Asmita Murumkar, Grey Evenson, Noel Aloysius, Richard Becker, Chelsie Boles, Remegio Confesor, Awoke Dagnew, Tian Guo, Rebecca Logsdon Muenich, Todd Redder, Yu-Chen Wang, and Donald Scavia. Using a Multi-Institutional Ensemble of Watershed Models to Assess Agricultural Conservation Effectiveness in a Future Climate. *JAWRA Journal of the American Water Resources Association*, 58(6):1326–1340, 2022. doi: https://doi.org/10.1111/1752-1688.13023. URL `https://onlinelibrary.wiley.com/doi/abs/10.1111/1752-1688.13023`. _eprint: https://onlinelibrary.wiley.com/doi/pdf/10.1111/1752-1688.13023.

Meongsu Lee, Wyatt Thompson, and Patrick Westhoff. The United States–China Trade War and Impact on the Post-Conservation Reserve Program Land Allocation. *Journal of Agricultural and Applied Economics*, 55(2):217–237, 2023. ISSN 1074-0708. doi: 10.1017/aae.2023.3. URL `https://www.cambridge.org/core/product/6869043D7474FD03BAA0B375BDFE1BC2`. Edition: 2023/05/15.

Jianguo Liu, Vanessa Hull, H. Charles J. Godfray, David Tilman, Peter Gleick, Holger Hoff, Clau-

dia Pahl-Wostl, Zhenci Xu, Min Gon Chung, Jing Sun, and Shuxin Li. Nexus approaches to global sustainable development. *Nature Sustainability*, 1(9):466–476, 2018.

Jing Liu, Laura Bowling, Christopher Kucharik, Sadia Jame, Uris Baldos, Larissa Jarvis, Navin Ramankutty, and Thomas Hertel. Tackling policy leakage and targeting hotspots could be key to addressing the 'Wicked'challenge of nutrient pollution from corn production in the US. *Environmental Research Letters*, 18(10):105002, 2023. ISBN: 1748-9326 Publisher: IOP Publishing.

Scott M. Lundberg and Su-In Lee. A unified approach to interpreting model predictions. *Advances in neural information processing systems*, 30, 2017.

Alex L. Marten, Richard Garbaccio, and Ann Wolverton. Exploring the General Equilibrium Costs of Sector-Specific Environmental Regulations. *Journal of the Association of Environmental and Resource Economists*, 6(6):1065–1104, 2019.

Jay F. Martin, Margaret M. Kalcic, Noel Aloysius, Anna M. Apostel, Michael R. Brooker, Grey Evenson, Jeffrey B. Kast, Haley Kujawa, Asmita Murumkar, and Richard Becker. Evaluating management options to reduce Lake Erie algal blooms using an ensemble of watershed models. *Journal of Environmental Management*, 280:111710, 2021. ISBN: 0301-4797 Publisher: Elsevier.

Malte Meinshausen, S. J. Smith, K. Calvin, J. S. Daniel, M. L. T. Kainuma, J-F. Lamarque, K. Matsumoto, S. A. Montzka, S. C. B. Raper, K. Riahi, A. Thomson, G. J. M. Velders, and D.P. P. van Vuuren. The RCP greenhouse gas concentrations and their extensions from 1765 to 2300. *Climatic Change*, 109(1):213, 2011.

Joshua P. Newell, Benjamin Goldstein, and Alec Foster. A 40-year review of food-energy-water nexus literature and its application to the urban scale. *Environmental Research Letters*, 14(7): 073003, 2019.

Brian C. O'Neill, Timothy R. Carter, Kristie Ebi, Paula A. Harrison, Eric Kemp-Benedict, Kasper Kok, Elmar Kriegler, Benjamin L. Preston, Keywan Riahi, Jana Sillmann, Bas J. van

Ruijven, Detlef van Vuuren, David Carlisle, Cecilia Conde, Jan Fuglestvedt, Carole Green, Tomoko Hasegawa, Julia Leininger, Seth Monteith, and Ramon Pichs-Madruga. Achievements and needs for the climate change scenario framework. *Nature Climate Change*, 10 (12):1074–1084, December 2020. ISSN 1758-6798. doi: 10.1038/s41558-020-00952-0. URL https://doi.org/10.1038/s41558-020-00952-0.

A. V. Pastor, A. Palazzo, P. Havlik, H. Biemans, Y. Wada, M. Obersteiner, P. Kabat, and F. Ludwig. The global nexus of food-trade-water sustaining environmental flows by 2050. *Nature Sustainability*, 2(6):499–507, 2019.

Janine Pelikan, Wolfgang Britz, and Thomas W. Hertel. Green Light for Green Agricultural Policies? An Analysis at Regional and Global Scales. *Journal of Agricultural Economics*, 66(1): 1–19, 2015.

Reinhard Prestele, Almut Arneth, Alberte Bondeau, Nathalie de Noblet-Ducoudré, Thomas A. M. Pugh, Stephen Sitch, Elke Stehfest, and Peter H. Verburg. Current challenges of implementing anthropogenic land-use and land-cover change in models contributing to climate change assessments. *Earth System Dynamics*, 8(2):369–386, May 2017. ISSN 2190-4979. doi: 10.5194/esd-8-369-2017. URL https://esd.copernicus.org/articles/8/369/2017/esd-8-369-2017.html. Publisher: Copernicus GmbH.

Anita Regmi. Retaliatory tariffs and U.S. agriculture. CRS Report R45903, Congressional Research Service, September 2019. URL https://www.everycrsreport.com/files/20190913_R45903_7cbb5ba8d2382a6472ca2eab14988a177063e19d.pdf.

Keywan Riahi, Detlef P. van Vuuren, Elmar Kriegler, Jae Edmonds, Brian C. O'Neill, Shinichiro Fujimori, Nico Bauer, Katherine Calvin, Rob Dellink, Oliver Fricko, Wolfgang Lutz, Alexander Popp, Jesus Crespo Cuaresma, Samir Kc, Marian Leimbach, Leiwen Jiang, Tom Kram, Shilpa Rao, Johannes Emmerling, Kristie Ebi, Tomoko Hasegawa, Petr Havlik, Florian Humpenöder, Lara Aleluia Da Silva, Steve Smith, Elke Stehfest, Valentina Bosetti, Jiyong Eom, David Ger-

naat, Toshihiko Masui, Joeri Rogelj, Jessica Strefler, Laurent Drouet, Volker Krey, Gunnar Luderer, Mathijs Harmsen, Kiyoshi Takahashi, Lavinia Baumstark, Jonathan C. Doelman, Mikiko Kainuma, Zbigniew Klimont, Giacomo Marangoni, Hermann Lotze-Campen, Michael Obersteiner, Andrzej Tabeau, and Massimo Tavoni. The Shared Socioeconomic Pathways and their energy, land use, and greenhouse gas emissions implications: An overview. *Global Environmental Change*, 42:153–168, 2017.

K. C. Samir and Wolfgang Lutz. The human core of the shared socioeconomic pathways: Population scenarios by age, sex and level of education for all countries to 2100. *Global Environmental Change*, 42:181–192, 2017. ISBN: 0959-3780 Publisher: Elsevier.

Gary Schnitkey. Anhydrous ammonia, corn, and natural gas prices over time. *farmdoc daily*, 6, 2016.

USEPA. U.S. Action Plan for Lake Erie. Technical report, U.S. Environmental Protection Agency, February 2018. URL `https://www.epa.gov/glwqa/us-action-plan-lake-erie`.

Detlef P. Van Vuuren, David L. Bijl, Patrick Bogaart, Elke Stehfest, Hester Biemans, Stefan C. Dekker, Jonathan C. Doelman, David E. H. J. Gernaat, and Mathijs Harmsen. Integrated scenarios to support analysis of the food-energy-water nexus. *Nature Sustainability*, 2(12):1132–1141, 2019.

Peter H Verburg, Peter Alexander, Tom Evans, Nicholas R Magliocca, Ziga Malek, Mark DA Rounsevell, and Jasper van Vliet. Beyond land cover change: towards a new generation of land use models. *Current Opinion in Environmental Sustainability*, 38:77–85, June 2019. ISSN 1877-3435. doi: 10.1016/j.cosust.2019.05.002. URL `https://www.sciencedirect.com/science/article/pii/S1877343518301362`.

Aaron B. Wilson, Alvaro Avila-Diaz, Lais F. Oliveira, Cristian F. Zuluaga, and Bryan Mark. Climate extremes and their impacts on agriculture across the Eastern Corn Belt Region of the US. *Weather and Climate Extremes*, 37:100467, 2022. ISBN: 2212-0947 Publisher: Elsevier.

Appendix

A Recursive Dynamic CGE Model

The recursive dynamic CGE model consists of two separate models: a dynamic regional model and a five-state static CGE model. Instead of listing all equations for both models, this section describes the equations of the recursive dynamic CGE model as if it is a single model. It should be noted that the transition laws for state variables (e.g., fossil fuel extraction, electricity generation capacity evolution, and industry capital stock evolution) are the parts of the dynamic regional model. The relevant intertemporal decisions (e.g., investment in a certain type of electricity generation capacity) are decided in the regional model and then allocated to each state in the state-level model by their shares of corresponding capital stocks in the region.

A.1 The Household

The representative household in each state, j, and in period, t, maximizes their utility given their budget constraint. The utility function is a function of a consumption bundle, $\mathbf{y}_t = (y_t^{food}, y_t^{energy}, y_t^{gas,heat}, y_t^{general})$, of the consumption of foods y_t^{food} , energy services y_t^{energy}, gas for heating $y_t^{gas,heat}$, general goods and services $y_t^{general}$:

$$U(\mathbf{y}_t^j) \cdot Pop_t^j \tag{A.1}$$

and the additively separable utility function is defined as

$$U(\mathbf{y_t}) = \frac{\left(y_t^{general}\right)^{1-\gamma_c^{manu}}}{1-\gamma_c^{general}} + \omega^{food}\frac{\left(y_t^{food}\right)^{1-\gamma_c^{food}}}{1-\gamma_c^{food}} + \omega^{energy}\frac{\left(y_t^{energy}\right)^{1-\gamma_c^{energy}}}{1-\gamma_c^{energy}} + \omega^{trans}\frac{\left(y_t^{gas,heat}\right)^{1-\gamma_c^{gas}}}{1-\gamma_c^{gas}} \tag{A.2}$$

for each period t, where ω are weights assigned to each consumption goods and γ_c are a parameter associated with the degree of relative risk aversion.

The energy services is a composite of electricity $y_t^{energy,elec}$ and transportation energy, $y_t^{energy,trans}$,

and is expressed as

$$y_t^{energy} = \left[\phi^{energy}\left(y_t^{energy,elec}\right)^{\rho_e} + (1-\phi^{energy})\left(y_t^{energy,trans}\right)^{\rho_e}\right]^{\frac{1}{\rho_e}} \tag{A.3}$$

where ϕ^{energy} denotes the share of energy service provided by electricity and σ_e is the elasticity of substitution between two energy services ($\sigma_e = \frac{1}{1-\rho_e}$).

In each period t, the household maximizes their utility given the following budget constraint:

$$\Pi_t^{Total,j} + \sum_{cap} \kappa^j K_t^{cap,j} + \sum_{ld} \iota_t^{ld,j} L_t^{ld} + \sum_{lb} w_t^{lb,j} N_t^{lb} \tag{A.4}$$

$$= Pop_t^j \cdot \left(\sum p^{con} y_t^{con}\right) + \sum I_t^{cap} + \sum_{ff} \zeta_t^{CCS,ff} + \zeta_t^{DAC} \tag{A.5}$$

. The left hand side shows the total income earned that is the sum of the profits from firms ($\Pi_t^{Total,j}$) and the returns on capital ($\sum_{cap} \kappa^j K_t^{cap,j}$) and on land ($\sum_{lb} w_t^{lb,j} L_t^{lb}$), given the assumption that the household owns the firms, land, and capital in the economy. The total profits from firms, $\Pi_t^{Total,j}$, is the sum of profits from each firm. cap indicates sectors using a capital input, $cap \in \{elec.coal, elec.gas, elec.wind, elec.solar, general\}$, ld indicates sectors using land as an input, $ld \in \{corn, soy, wheat, specialty, livestock\}$, and lb indicates sectors taking labor input, $lb \in \{corn, soy, wheat, specialty, livestock, food, elec.coal, elec.gas, elec.wind, transportation\}$. κ, ι, and w represent return rates for capital and land, and wage for each sector in each state, respectively. The right hand side shows the total spending in consumption of goods and services ($Pop_t^j \cdot (\sum p^{con} y_t^{con})$), capital investment ($\sum I_t^{cap}$), and operation cost of carbon capture ($\sum_{ff} \zeta_t^{CCS,ff}$) and direct air capture (ζ_t^{DAC}). con indicates consumption goods, $con \in \{food, energy, gas, general\}$. In the following, the state index, j, is omitted as equations are symmetric across the five states.

A.2 Agricultural and Food Sector

A.2.1 Crop Farm

The Q_t^{crop} amount of a crop is produced using L_t^{crop} of land, F_t^{crop} of fertilizer, and N_t^{crop} of labor for each crop ($crop \in \{corn, soy, wheat, specialty\}$). Given that, the the firm's profit is defined as the revenue from selling crops net of input costs:

$$\begin{aligned}\Pi_t^{crop} =& p_t^{crop} Q_t^{crop} \\ & - p_t^{fert,crop} F_t^{crop} - w_t N_t^{crop} - \iota_t L_t^{crop}\end{aligned}$$

where p_t^{crop} is a crop price and $p_t^{fert,crop}$ is crop-specific fertilizer price in each state. The profit is maximized given the crop production technology feasibility constraint. The crop production function is a nested normalized constant elasticity of substitution (CES) function of the three inputs,

$$\begin{aligned}\frac{Q_t^{crop}}{Q_0^{crop}} = A_t^{crop} \Bigg[(1-\beta^{crop}) \Bigg\{ \omega^{crop} \left(\frac{L_t^{crop}}{L_0^{crop}} \right)^{\rho^{1,crop}} + (1-\omega^{crop}) \left(\frac{F_t^{crop}}{F_0^{crop}} \right)^{\rho^{1,crop}} \Bigg\}^{\frac{\rho^{2,crop}}{\rho^{1,crop}}} \\ + \beta^{crop} \left(\frac{N_t^{crop}}{N_0^{crop}} \right)^{\rho^{2,crop}} \Bigg]^{\frac{\alpha^{crop}}{\rho^{2,crop}}}\end{aligned} \tag{A.6}$$

where A_t^{crop} is the crop-specific total factor productivity and α^{crop} is a decreasing returns to scale parameter in the region.

A.2.2 Livestock Farm

The livestock products, $Q_t^{livestock}$, are produced with crop feeds of corn $Q_t^{corn,feed}$ and soybean $Q_t^{soy,feed}$, the labor $N_t^{livestock}$, and the pasture land $L_t^{pasture}$. The profit is maximized:

$$\begin{aligned}\Pi_t^{livestock} =& p^{livestock} Q_t^{livestock} \\ & - p_t^{corn} Q_t^{corn,feed} - p_t^{soy} Q_t^{soy,feed} - w_t N_t^{livestock} - \iota_t L_t^{pasture}\end{aligned} \tag{A.7}$$

The livestock production function is formulated as a Cobb-Douglas function,

$$\frac{Q_t^{livestock}}{Q_0^{livestock}} = A_t^{livestock} \left(\frac{Q_t^{corn,feed}}{Q_0^{corn,feed}} \right)^{\alpha^l} \left(\frac{Q_t^{soy,feed}}{Q_0^{soy,feed}} \right)^{\beta^l} \left(\frac{N_t^{livestock}}{N_0^{livestock}} \right)^{\eta^l} \left(\frac{L_t^{pasture}}{L_0^{pasture}} \right)^{\gamma^l} \tag{A.8}$$

where $A_t^{livestock}$ is the total factor productivity for livestock production. The parameters α^l, β^l, η^l, and γ^l are share parameters and their sum is assumed to be less than one.

A.2.3 Food Production Firm

The Y_t^{food} amount of food is produced with $Q_t^{corn,food}$, $Q_t^{soy,food}$, $Q_t^{wheat,food}$, $Q_t^{specialty,food}$, and $Q_t^{livestock,food}$ of corn, soybeans, wheat, specialty crops, and livestock products, respectively, and the N_t^{food} amount of labor. Thus, the profit is expressed:

$$\begin{aligned} \Pi_t^{food} =& p^{food} Y_t^{food} \\ & - p_t^{corn} Q_t^{corn,food} - p_t^{soy} Q_t^{soy,food} - p_t^{wheat} Q_t^{wheat,food} - p_t^{specialty} Q_t^{specialty,food} \\ & - p_t^{livestock} Q_t^{livestock,food} - w_t N_t^{food} \end{aligned} \tag{A.9}$$

The food production function has a nested structure, where, first, a non-meat food composite and meat production are combined in a CES function, which then comprises a Cobb-Douglas function with the labor input:

$$\begin{aligned} \frac{Y_t^{food}}{Y_0^{food}} = & \left[\left(1 - \omega_t^{f5}\right) \left\{ \left(\frac{Q_t^{corn,food}}{Q_0^{corn,food}} \right)^{\omega^{f1}} \left(\frac{Q_t^{soy,food}}{Q_0^{soy,food}} \right)^{\omega^{f2}} \left(\frac{Q_t^{wheat}}{Q_0^{wheat}} \right)^{\omega^{f3}} \left(\frac{Q_t^{specialty,food}}{Q_0^{specialty,food}} \right)^{\omega^{f4}} \right\}^{\alpha^f} \right. \\ & \left. + \omega_t^{f5} \left(\frac{Q_t^{livestock,food}}{Q_0^{livestock,food}} \right)^{\alpha^f} \right]^{\frac{\beta^f}{\alpha^f}} \left[\frac{N_t^{food}}{N_0^{food}} \right]^{1-\beta^f} \end{aligned} \tag{A.10}$$

where ω^{f1}, ω^{f2}, ω^{f3}, and ω^{f4} are the shares of corn, soybeans, wheat, and specialty crops in the non-meat food composite, respectively, (with $\omega^{f1} + \omega^{f2} + \omega^{f3} + \omega^{f4} = 1$), and ω_t^{f5} represents a share parameter associated with meat consumption and its trend representing a diet pattern

change.β^f indicates the share of labor input in food production. α^f is a substitution elasticity parameter.

A.3 Energy Sector

A.3.1 Fossil Fuel Extraction Firm

Fossil fuels are extracted (D_t^{ff}) from finite recoverable reserves and the stock remaining at time t is R_t^{ff}. Each resource stock R_t^{ff} satisfies the following stock transition law:

$$R_{t+1}^{ff} = R_t^{ff} - D_t^{ff} \tag{A.11}$$

where D_t^{ff} is the extracted amount of coal or natural gas ($ff \in \{coal, gas\}$). The extraction cost functions of coal and natural gas are

$$G^{ff} = \theta^{ff} \left(\frac{D_t^{ff}}{R_t^{ff}} \right)^{\alpha_{ff}} + \left(reg_t^{ff} + \tau_t^{ff,co_2} \right) D_t^{ff} \tag{A.12}$$

where reg_t^{ff} is the annual cost spent to meet current regulation standards and only applies to coal, and τ_t^{ff,co_2} is the potential global-level carbon tax imposed on the fossil fuels supplied to the regional economy. The profit function is

$$\Pi_t^{ff} = p_t^{ff} D_t^{ff} - G_t^{ff} \tag{A.13}$$

A.3.2 Fossil Fuel Electricity Generation Firm

The fossil fuel-fired electricity generation, $E_t^{elec,ff}$, takes the inputs of corresponding fossil fuel, $D_t^{ff,elec}$, generation capacity, $K_t^{elec,ff}$, and labor, $N_t^{elec,ff}$. The firm's profit is

$$\Pi_t^{elec,ff} = p^{elec} E_t^{elec,ff} - p_t^{ff} D_t^{ff,elec} - \iota_t^{elec,ff} K_t^{elec,ff,total} - w_t N_t^{elec,ff} \tag{A.14}$$

. Its production function is formulated as a CES function:

$$\frac{E_t^{elec,ff}}{E_0^{elec,ff}} = A_t^{elec,ff}\left[\omega^{elec,ff}\left(\frac{K_t^{elec,ff,total}}{K_0^{elec,ff,total}}\right)^{\alpha^{elec,ff}} + \left(1-\omega^{elec,ff}\right)\left(\frac{D_t^{ff,elec}}{D_0^{ff,elec}}\right)^{\alpha^{elec,ff}}\right]^{\frac{1-\beta^{elec,ff}}{\alpha^{elec,ff}}} \cdot \left(\frac{N_t^{elec,ff}}{N_0^{elec,ff}}\right)^{\beta^{elec,ff}} \tag{A.15}$$

The fossil-based power plant technologies considered in the model include ultra-supercritical (USC) coal plant (*coal*), USC coal plant with 90% sequestration (*coal*90), combined cycle - single shaft natural gas plant (*gas*), and combined cycle plant with 90% sequestration (*gas*90). To incorporate two types of plant technology for each fossil fuel, we assume: 1) the labors and fossil fuels are able to move freely across different technology power plants (that is, only one aggregate labor, fossil fuel input, and generation quantity for each fuel type), 2) each plant always operates to its full capacity (no under-utilization), and 3) greenhouse gas emissions calculation is based on the capacity share of each technology type using the same fossil fuel.

The total capacity of fossil fuel-fired electricity generation for each fuel is the sum of power plant capacity with and without CCS:

$$K_t^{elec,ff,total} = K_t^{elec,ff} + K_t^{elec,ff_{seq}} \tag{A.16}$$

where $ff_{seq} \in \{coal90, gas90\}$. The capital transition law is specific to a plant type.

The plant capacity without CCS depreciates with the rate of $\delta^{elec,ff}$, grows with the addition of new capacity, $I_t^{elec,ff}/p_t^{elec,ff}$, net of the capacity retrofitted into a plant with CCS, $I_t^{elec,ff_{retro}}/p_t^{elec,ff_{retro}}$ (A.3.2). The plant capacity with CCS also depreciates with the rate of $\delta^{elec,ff}$, grows with the addition of new capacity, $I_t^{elec,ff_{seq}}/p_t^{elec,ff_{seq}}$ and the capacity retrofitted from a plant without CCS, $I_t^{elec,ff_{retro}}/p_t^{elec,ff_{retro}}$ (A.3.2). I^{ff} and p^{ff} represent the plant-specific investment in dollar value and their associated overnight capital investment costs, respectively, and their division translates

into new capacity addition.

$$K_{t+1}^{elec,ff} = \left(1-\delta^{elec,ff}\right) K_t^{elec,ff} + I_t^{elec,ff}/p_t^{elec,ff} - I_t^{elec,ff_{retro}}/p_t^{elec,ff_{retro}} \tag{A.17}$$

$$K_{t+1}^{elec,ff_{seq}} = (1-\delta^{elec,ff}) K_t^{elec,ff_{seq}} + I_t^{elec,ff_{seq}}/p_t^{elec,ff_{seq}} + I_t^{elec,ff_{retro}}/p^{elec,ff_{retro}} \tag{A.18}$$

The operational costs for coal and gas power plants with 90% sequestration are:

$$\zeta_t^{CCS,ff} = \theta^{ff} \times 90\% \times CO_2 factor_t^{elec,ff} E_t^{elec,ff} \left(\frac{K_t^{elec,ff_{seq}}}{K_t^{elec,ff,total}}\right) \tag{A.19}$$

where θ^{ff} is the CO_2 capture cost per metric ton for each plant type and $CO_2 factor^{elec,ff}$ is the average emissions rate of CO_2 per terawatt-hour (TWh).

A.3.3 Renewable Electricity Generation Firm

The renewable electricity, $E_t^{elec,renew}$, is assumed to take the renewable electricity generation capacity, $K_t^{elec,renew}$, as the major input and the rest inputs are implicitly incorporated in the total factor productivity. The firm's profit is

$$\Pi_t^{elec,renew} = p^{elec} E_t^{elec,renew} - \iota_t^{elec,ff} K_t^{elec,ff,total} \tag{A.20}$$

The production function of renewable electricity is

$$\frac{E_t^{elec,renew}}{E_0^{elec,renew}} = A_t^{elec,renew} \left(\frac{K_t^{elec,renew}}{K_0^{elec,renew}}\right)^{\alpha_{elec,renew}} \tag{A.21}$$

and the capacity transition law follows

$$K_{t+1}^{elec,renew} = \left(1-\delta^{elec,renew}\right) K_t^{elec,renew} + I_t^{elec,renew}/p_t^{elec,renew} \tag{A.22}$$

A.4 Transportation Energy Services Firm

The transportation energy is supplied by four types of energy sources: gasoline $D_t^{oil,gasoline}$, diesel $D_t^{oil,diesel}$, corn-based ethanol $Q_t^{corn,trans}$, and electricity $E_t^{trans,elec}$. The firm's profit is expressed:

$$\begin{aligned}\Pi_t^{trans} =& p^{trans}E_t^{trans} - p_t^{oil}\left(D_t^{oil,gasoline} + D_t^{oil,diesel}\right) \\ & - p_t^{corn}Q_t^{corn,trans} - p_t^{elec}E_t^{trans,elec} - w_t N_t^{trans}\end{aligned} \tag{A.23}$$

The production function is constructed as a nested CES function, with the outer nest composed of the electricity energy and non-electricity combustion-based energy, and then with the inner one characterized with the substitution between diesel, gasoline and fuel ethanol.

$$\frac{E_t^{trans}}{E_0^{trans}} = A_t^{trans}\left[\omega^{elec}\left(\frac{E_t^{trans,elec}}{E_0^{trans,elec}}\right)^{\alpha^{trans}} + (1-\omega^{elec})\left(\frac{E_t^{trans,combustion}}{E_0^{trans,combustion}}\right)^{\alpha^{trans}}\right]^{\frac{\gamma^{trans}}{\alpha^{trans}}}\left(\frac{N_t^{trans}}{N_0^{trans}}\right)^{\eta^{trans}} \tag{A.24}$$

where

$$\begin{aligned}\frac{E_t^{trans,combustion}}{E_0^{trans,combustion}} = & \left[\omega^{diesel}\left(\frac{D_t^{oil,diesel}}{D_0^{oil,diesel}}\right)^{\alpha^{oil}}\right. \\ & \left. + \left(1-\omega^{diesel}\right)\left(\omega^{gasoline}\left(\frac{D_t^{oil,gasoline}}{D_0^{oil,gasoline}}\right)^{\rho^{oil}} + \left(1-\omega^{gasoline}\right)\left(\frac{Q_t^{corn,trans}}{Q_0^{corn,trans}}\right)^{\rho^{oil}}\right)^{\frac{\alpha^{oil}}{\rho^{oil}}}\right]^{\frac{1}{\alpha^{oil}}}\end{aligned} \tag{A.25}$$

. In terms of electricity energy, it is assumed that the efficiency of conversion of electricity energy to vehicle miles traveled continues to improve through 2050. The trend is expressed with the equation for the effective energy provided by electricity

$$E_t^{trans,elec} = \gamma_t^{elec,efficiency}E_t^{trans,elec,raw} \tag{A.26}$$

and the efficiency parameter $\gamma_t^{elec,ef}$ for the electricity energy for transportation, which is assumed

to linearly increase to reach 4 times relative to fossil-fuel energy until 2050 for T (=35) years:

$$\gamma_{t\leq T}^{elec,efficiency} = 1 + \frac{3}{T-1}(t-1) \tag{A.27}$$

$$\gamma_{t>T}^{elec,ef} = 4 \tag{A.28}$$

A.5 General Goods and Services Production

The general goods and services production, which accounts for the aggregate of the rest of regional GDP, takes capital $K_t^{general}$, electricity $E_t^{general,elec}$, transportation energy $E_t^{general,trans}$, and labor $N_t^{general}$ to produce $Y_t^{general}$. As this product is designated as a numeraire in the model, its price is set to one. Its profit is

$$\begin{aligned}\Pi_t^{general} =& Y_t^{general} - \kappa K_t^{general} \\ & - p_t^{trans} E_t^{general,trans} - p_t^{elec} E_t^{general,elec} - w_t N_t^{general}\end{aligned} \tag{A.29}$$

. The production function is

$$\begin{aligned}\frac{Y_t^{general}}{Y_0^{general}} = A_t^{general} \Bigg[& \phi^K \left(\frac{K_t^{general}}{K_0^{general}} \right)^{\rho_m} \\ & + \left(1-\phi^K\right) \Bigg[\phi^m \left(\frac{E_t^{general,elec}}{E_0^{general,elec}} \right)^{\rho_{energy}} + (1-\phi^m) \left(\frac{E_t^{general,trans}}{E_0^{general,trans}} \right)^{\rho_{energy}} \Bigg]^{\frac{\rho_m}{\rho_{energy}}} \Bigg]^{\frac{\alpha_{ke}}{\rho_m}} \left(\frac{N_t^{general}}{N_0^{general}} \right)^{1-\alpha_{ke}}\end{aligned} \tag{A.30}$$

. Its capital follows the transition law of

$$K_{t+1}^{general} = (1-\delta) K_t^{general} + I_t^{general} \tag{A.31}$$

.

A.6 Trading Firm

Assume that each state has a single representative trading firm and its profit is generated by the differences between a trade price and a state market price, net of transaction costs:

$$
\begin{aligned}
\Pi_t^{trade,j} = \sum_{crop} \Bigg\{ & \left[\left(1 - TC^{crop,j}\right) p_t^{crop,trade} - p_t^{crop,j} \right] Q_t^{crop,ex} \\
& + \left[p_t^{crop,j} - \left(1 + TC^{crop,j}\right) p_t^{crop,trade} \right] Q_t^{crop,im} \Bigg\} \\
& + \left[\left(1 - TC^{livestock,j}\right) p_t^{livestock,trade} - p_t^{livestock,j} \right] Q_t^{livestock,ex} \\
& + \left[p_t^{livestock,j} - \left(1 + TC^{livestock,j}\right) p_t^{livestock,trade} \right] Q_t^{livestock,im} \\
& + \left[\left(1 - TC^{elec,j}\right) p_t^{elec,trade} - p_t^{elec,j} \right] E_t^{elec,ex} \\
& + \left[p_t^{elec,j} - \left(1 + TC^{elec,j}\right) p_t^{elec,trade} \right] E_t^{elec,im} \\
& + \left[\left(1 - TC^{gas,j}\right) p_t^{gas,trade} - p_t^{gas,j} \right] D_t^{gas,ex} \\
& + \left[p_t^{gas,j} - \left(1 + TC^{gas,j}\right) p_t^{gas,trade} \right] D_t^{gas,im} \\
& + \left[\left(1 - TC^{coal,j}\right) p_t^{coal,trade} - p_t^{coal,j} \right] D_t^{coal,ex} \\
& + \left[p_t^{coal,j} - \left(1 + TC^{coal,j}\right) p_t^{coal,trade} \right] D_t^{coal,im} \\
& + \left[p_t^{oil,j} - \left(1 + TC^{oil,j}\right) p_t^{oil,trade} \right] D_t^{oil,im}
\end{aligned}
\tag{A.32}
$$

where TC represent product- and state-specific transaction costs.

A.7 Market Clearing

A.7.1 Agricultural and Food Sector

The produced and imported corn is used for producing food, feeding livestock, generating corn-based ethanol fuel, and exporting:

$$Q^{corn} + Q^{corn,im} = Q^{corn,food} + Q^{corn,feed} + Q^{corn,trans} + Q^{corn,ex} \tag{A.33}$$

The produced and imported soybean is used for producing food, feeding livestock, and exporting:

$$Q^{soy} + Q^{soy,im} = Q^{soy,food} + Q^{soy,feed} + Q^{soy,ex} \tag{A.34}$$

The produced and imported wheat is used for producing food and exporting:

$$Q^{wheat} + Q^{wheat,im} = Q^{wheat,food} + Q^{wheat,ex} \tag{A.35}$$

The produced and imported specialty crops are used for producing food and exporting:

$$Q_t^{specialty} + Q_t^{specialty,im} = Q_t^{specialty,food} + Q_t^{specialty,ex} \tag{A.36}$$

The produced and imported livestock is used for producing food and exporting:

$$Q_t^{livestock} + Q_t^{livestock,im} = Q_t^{livestock,food} + Q_t^{livestock,ex} \tag{A.37}$$

We assume that all produced food is consumed by the household:

$$Y_t^{food} = y_t^{food} pop_t \tag{A.38}$$

The total amount of land inputs for agricultural sectors and ecosystem services sum to the total

available land in the region:

$$L_t^{total} = L_t^{corn} + L_t^{soy} + L_t^{wheat} + L_t^{specialty} + L_t^{pasture} + L_t^{eco} \tag{A.39}$$

where L_t^{total} is exogenous.

A.7.2 Energy Sector

The total production of electricity from fossil fuels, renewables and other resources equal the electricity used in manufacturing firms plus the electricity used by the household:

$$\begin{aligned} &\sum_{ff} E_t^{elec,ff} + \sum_{ff_{seq}} E_t^{elec,ff_{seq}} + \sum_{renew} E_t^{elec,renew} + E_t^{elec,im} + E_t^{other} \\ &\quad = y_t^{energy,elec} pop_t + E_t^{general,elec} + E_t^{trans,elec,raw} + E_t^{elec,ex} \end{aligned} \tag{A.40}$$

The total produced transportation energy is consumed by the manufacturing firms and the household:

$$E_t^{trans} = E_t^{general,trans} + y_t^{energy,trans} pop_t \tag{A.41}$$

The total amount of coal extracted and imported equals the coal used in electricity and exporting:

$$D_t^{coal} + D_t^{coal,im} = D_t^{coal,elec} + D_t^{coal,ex} \tag{A.42}$$

The total amount of natural gas extracted and imported equals the natural gas used in electricity and heating service used by the households and exported:

$$D_t^{gas} + D_t^{gas,im} = D_t^{gas,elec} + y_t^{energy,gas} pop_t + D_t^{gas,ex} \tag{A.43}$$

The total amount of the imported oil equals the total amount of diesel and gasoline used in the

transportation energy firms:

$$D_t^{oil,im} = D_t^{diesel} + D_t^{gasoline} \tag{A.44}$$

A.7.3 Labor Market

$$\begin{aligned} N_t^{total} =& N_t^{corn} + N_t^{soy} + N_t^{wheat} + N_t^{specialty} + N_t^{livestock} + N_t^{food} + \\ & N_t^{general} + N_t^{trans} + N_t^{elec,coal} + N_t^{elec,gas} \end{aligned} \tag{A.45}$$